Glutathione-mediated thermomorphogenesis and heat stress responses in Arabidopsis thaliana

Avilien Dard, Alizée Weiss, Laetitia Bariat, Juline Auverlot, Valentine Fontaine, Nathalie Picault, Frédéric Pontvianne, Christophe Riondet, Jean-Philippe Reichheld

Glutathione-mediated thermomorphogenesis and heat stress responses in *Arabidopsis thaliana*

Avilien Dard[1,2], Alizée Weiss[1,2], Laetitia Bariat[1,2], Juline Auverlot[1,2], Valentine Fontaine[1,2], Nathalie Picault[1,2], Frédéric Pontvianne[1,2], Christophe Riondet[2,1], Jean-Philippe Reichheld[1,2*]

[1] Laboratoire Génome et Développement des Plantes, Université Perpignan Via Domitia, F-66860 Perpignan, France

[2] Laboratoire Génome et Développement des Plantes, CNRS, F-66860 Perpignan, France

[*] To whom correspondence should be addressed: E-mail: jpr@univ-perp.fr.

Jean-Philippe Reichheld, Tel: +33 4 68662225; Fax: +33 4 68668499; E-mail: jpr@univ-perp.fr. Laboratoire Génome et Développement des Plantes, Université Perpignan Via Domitia, F-66860 Perpignan, France.

Highlights: Arabidopsis plants with low glutathione levels failed to induce thermomorphogenesis and are susceptible to heat stress.

Abstract

In the context of climate change, the global rise of temperature and intense heat waves affect plant development and productivity. Among the molecular perturbations that high temperature induces in living cells is the accumulation of reactive oxygen species (ROS), which perturbs the cellular redox state. In plants, the dynamics of the cellular and subcellular redox state has been poorly investigated under high temperature. Glutathione plays a major role in maintaining the cellular redox state. We investigated its contribution in adaptation of *Arabidopsis thaliana* to contrasted high temperature regimes, high ambient temperature inducing thermomorphogenesis and heat stress affecting plant viability. Using the genetically- encoded redox marker roGFP2, we show that high temperature regimes lead to cytoplasmic and nuclear oxidation and impact the glutathione pool. This pool is restored within a few hours, which likely contributes to plant adaptation to high temperatures. Moreover, low glutathione mutants fail to adapt to heat stress and to induce thermomorphogenesis, suggesting that glutathione is involved in both heat adaptation mechanisms. We also evaluate the transcriptomic signature in the two high temperature regimes and identified gene expression deviations in low glutathione mutants, which might contribute to their sensitivity to high temperature. Thus, we define glutathione as a major actor in the adaptation of the plant to contrasting high temperature regimes.

Keywords: Antioxidant; Glutathione; Heat; Redox; ROS; Stress; Temperature; Thermomorphogenesis; Thermotolerance; Arabidopsis.

Introduction

Climate change leads to a global warming of the earth's temperature and induces more frequent and intense heat waves which impact sustainable plant yield (Liu *et al.*, 2016; Bailey-Serres et al., 2019; IPCC, 2021). During periods of heat stress, living organisms need to rapidly adapt to cope with the damaging effects of increasing temperatures. However, the mechanisms involved in the adaptation to heat stress largely differ depending on the duration and intensity of the stress. In Arabidopsis, for which optimal temperature growth is generally established at 20-22°C, an intense rise in temperatures (e.g. 35-42°C) often found during summer heat waves can be harmful to cellular macromolecules like lipids and proteins. Extreme heat temperatures particularly impact the early stages of plant development like seed germination, radicle emergence and seedling growth (Toh et al., 2008) as well as reproductive organs, causing flower abortion and decreased pollen germination (Sato et al., 2006). Heat stress also impacts photosynthesis efficiency, as different key enzymes like the Rubisco and the Rubisco activase are heat sensitive (Portis et al., 2003) as well as starch and sucrose synthase (Sumesh et al., 2008). The impact of heat stress on membrane fluidity also destabilizes chloroplastic and mitochondrial electron transport chains (ETC), leading to loss of energy and release of reactive oxygen species (ROS) (Mittler et al., 2012; Choudhury *et al.*, 2017; Noctor et al., 2018). Upon heat stress, ROS are also generated at the plasma membrane/apoplast interface by NADPH oxidases, superoxide dismutases and peroxidases, and can be translocated to the cytosolic compartment by aquaporins, where they take part in stress signalling pathways (Mittler *et al.*, 2012; Rodrigues *et al.*, 2017; Mhamdi and Breusegem, 2018). Recently, the receptor kinase HPCA1 has been shown to sense H_2O_2 at the plasma membrane and to activate signalling cascades (Wu *et al.*, 2020). Another feature of the plant response to heat stress is a massive

reprogramming of the genome expression, which in Arabidopsis involves more than 25% of the total number of expressed genes (Merret et al., 2013). This reprogramming largely participates in the adaptation of the cell metabolism to this drastic environmental change. Among induced genes, many encode heat stress protection systems like heat shock factors (HSFs), heat shock proteins (HSPs) or ROS detoxification enzymes (Zandalinas et al., 2020). Also emphasizing the major contribution of ROS in heat stress signalling, ROS accumulation induces the expression of HSFs and HSPs. The activity of several HSFs like HSFA1 and HSF8 is indeed ROS dependent (Volkov et al., 2006; Giesguth et al., 2015; Delorme-Hinoux et al., 2016; Jacob et al, 2017; Martins et al., 2018).

Although the pathways regulating plant response to heat stress have been largely documented, the response mechanisms to high ambient temperatures such as 2-5°C above the optimal temperature range are less known. Physiologically, such regimes lead to developmental modifications like elongation of the hypocotyl, early flowering or modifications of stomata development, a process generically called thermomorphogenesis (Casal and Balasubramanian, 2019). Some molecular mechanisms underlying these developmental modifications have been investigated. They include gene expression reprogramming, chromatin remodelling or hormone accumulation (Casal and Balasubramanian, 2019). A network of transcriptional and posttranscriptional regulators involving the photoreceptor phytochrome B (PHYB) and the transcription factor PHYTOCHROME INTERACTING FACTOR 4 (PIF4) play a central role in inducing developmental promoting factors like auxins and brassinosteroids metabolism, flowering, or stomata development genes (Jung *et al.*, 2016; Legris *et al.*, 2016; Gangappa and Kumar, 2017). However, the contribution of ROS and antioxidant components in thermomorphogenesis is poorly documented.

Glutathione, as an important cellular antioxidant, is known to play key functions in many stress and developmental processes (Noctor et al., 2011; Foyer and Noctor, 2011; Considine and Foyer, 2014; Noctor et al., 2018). For example, the characterization of low glutathione mutants like *rootmeristemless1* (*rml1*), *cadmiumsensitive 2* (*cad2*) or phytoalexin-deficient mutant (*pad2*) have unravelled glutathione functions in tolerance to biotic and abiotic stresses and key plant developmental steps like shoot and root development (Cobbett *et al.*, 1998; Vernoux, 2000; Ball *et al.*, 2004; Parisy *et al.*, 2007; Reichheld *et al.*, 2007; Marty *et al.*, 2009; Bashandy *et al.*, 2010; Mhamdi *et al.*, 2010; Shanmugam *et al.*, 2012). However, its role in high temperature regimes like heat stress and thermomorphogenesis is poorly documented (Larkindale et al., 2005). Glutathione plays also an important role as a reductant, co-factor or substrate of many enzymes like glutaredoxins (GRXs), glutathione-S-transferases (GSTs) or peroxidases (PRXs) which might have functions in the response to high temperature (Noctor et al., 2011; Meyer et al., 2012). For example, the glutaredoxin GRXS17 has been documented as a redox-sensitive chaperone important in the tolerance to high temperature (Cheng et al., 2011; Wu et al., 2012; Martins et al., 2020).

By reacting with H_2O_2, reduced glutathione (GSH) is oxidized to GSSG, causing a shift of its redox potential (E_{GSH}) to less negative values. Thus, E_{GSH} is considered a good proxy to monitor cellular oxidation (Noctor et al., 2011). *In vivo* imaging techniques based on genetically-encoded redox-sensitive GFP (roGFP) sensors have been extensively used to monitor E_{GSH} in different mutants, stress or cell compartment contexts (Meyer et al., 2007; Gutcher et al., 2008; Schwarzländer et al., 2008; Marty et al., 2009; Babbar et al., 2021; Ugalde et al., 2022).

Here, we took advantage of the glutathione redox sensor GRX1-roGFP2 to explore the role of the maintenance of the cytosolic and nuclear glutathione redox state during heat stress and thermomorphogenesis. We define the level of glutathione as an important determinant for the tolerance to heat stress and establishment of the thermomorphogenesis. Finally, we delineate gene expression signatures induced by high temperature regimes in both wild-type and low glutathione mutants. The role of glutathione as an actor of genome expression adjustment upon heat stress is discussed.

Materials and Methods

Plant materials and growth conditions

Wild type (WT) *Arabidopsis thaliana* ecotype Columbia-0 (Col-0) and different mutants were used in this work: *cad2-1* (Howden *et al.*, 1995), *pad2-1* (Parisy *et al.*, 2007), *gr1-1* (Marty *et al.*, 2009), *cat2-1* (Queval *et al.*, 2007), *gsnor-1/hot5-2* (Lee *et al.*, 2008), *hsfA1QK* (Liu *et al.*, 2011; Yeh *et al.*, 2012), *grxc1* (Riondet *et al.*, 2012), *grxc2* (Riondet *et al.*, 2012), *pif4-2* (Koini *et al.*, 2009), *phyb*-9 (Reed *et al.*, 1993). *grxc3* and *grxc4* (Salk_062448 and Salk_128264) were ordered from the Nottingham Arabidopsis Stock Centre (NASC; http://arabidopsis.info/). PlaCCI seeds were provided by Bénédicte Desvoyes and Crisanto Gutierrez (Desvoyes *et al.*, 2020).

For in vitro plant culture, Arabidopsis seeds were surface-sterilized for 15 min with ethanol 70%, rinsed with ethanol 95% and completely dried before used. Sterilized seeds were plated on ½ MS agar medium (2.2 g/L Murashige and Skoog, 0.5 g/L MES, 0.5% plant agar (w/v), adjusted to pH 5.8) supplemented or not with buthionine sulfoximide (BSO,

Sigma-Aldrich) and stratified 48 h at 4°C in the dark. Seedlings were grown under 120 µmol.m^{-2}.s^{-1} photosynthetic flux at 20°C and the light cycle was 16 h light/8 h dark for long-day or 8 h light/16 h for short-day conditions. These growth conditions were systematically used unless otherwise indicated.

Thermotolerance assays

Seeds were first germinated at 20 °C, and after 4 to 7 days, seedlings were either transferred to 27 °C under short days (for thermomorphogenesis assays) or at 37°C under long-day conditions (for plant survival assays). Heat treatments were done by transferring plants in pre-heated MLR-352 Plant Growth Chambers (PHCbi, Sanyo). For thermomorphogenesis assays, pictures of each plate were taken and hypocotyls of at least 30 seedlings were measured using NIH ImageJ software with the NeuronJ plugin. For Thermotolerance to Moderate High Temperature (TMHT) experiments, the percentage of viability was calculated by counting the plants that recovered leaf growth 11 days after heat treatment. About 30 to 100 plants were used in each replicate for calculation and the mean was plotted ± SD at least 3 independent biological replicates.

Samples preparation and RNA-seq analysis

Seven days old seedlings were heated at 27°C or 37°C for 2h or 24h and control samples (20°C) were harvested just before the heat treatment. To take into account the contribution of the time of day and the circadian clock, heat stress treatments were done in the early morning, after 3h30 exposure to light (Blair *et al.*, 2019). For each condition, 3 biological replicates corresponding to different batches of plants were harvested and treated independently.

Each replicate was ground in liquid nitrogen with mortar and pestle and 100 mg of powder was used for RNA extraction using the Monarch® Total RNA Miniprep Kit. Briefly, the powder was suspended in an RNA protection reagent, vortexed and centrifuged for 2 min (16,000 x g). An equal volume of RNA Lysis buffer was mixed with the supernatant, loaded in the gDNA removal column and centrifuged for 2 min (16,000 x g). The flow-through was mixed with an equal volume of 100% ethanol. The mixture was then loaded into the RNA purification column, spun for 30 sec and incubated with DNase 1 for 15 min and washed with RNA priming buffer, RNA Wash buffer 2 times and RNA was eluted in 70 µl of nuclease-free water and kept at -80 °C. Next, 2 µg of total RNA was purified with Dynabeads Oligo-dT (25) and library quality was determined using Bio-Analyser 2100 (Agilent Genomics). Quantification was done using Q-BIT Qubit Fluorescence Reader (ThermoFisher Scientific) and replicates were then multiplexed with unique barcodes. Library amplification, RNA-sequencing and data analysis for each mRNA library, single-end 75 base pair sequences were sequenced using NextSeq 550 instrument (Illumina) at the Bio-environment platform, University of Perpignan Via Domitia (UPVD). Reads were trimmed using Trimmomatic (Bolger *et al.*, 2014), and mapped to the *A. thaliana* genome (Arabidopsis TAIR10 genome) using HISAT2 (Kim *et al.*, 2015). The sequence alignment files were sorted and indexed using SAMtools (Li *et al.*, 2009). The number of reads mapped onto a gene was calculated using HTSeq-count (Anders *et al.*, 2015). Differentially expressed genes were obtained with DESeq2 (Love *et al.*, 2014), using a log2 fold-change >1 (up-regulated genes) or < -1 (down-regulated genes) with an adjusted *p*-value of 0.01. PCA was realized using the PCA function from R. Heat map visualizations were realized using the heatmap2 function from the R ggplot2 package (Wickham, 2016).

Protein extraction, S-glutathionylation analysis and GST activity

For total protein extraction, about 1 g of 7 days-old seedlings was ground in liquid nitrogen with mortar and pestle and suspended in 250 µL of protein extraction buffer (25 mM Tris pH 7.6, 75 mM NaCl, 0.1 % NP40 with 1 tab/10 ml of complete protease inhibitor cocktail (Roche). The solution was vortexed, centrifuged (13 000 g, 20 min, 4 °C) and the supernatant was taken up and the protein concentration was determined using the Bradford assay (Biorad).

Proteins were heated for 3 min at 95 °C in a non-reducing Leammli buffer (62.5 mM Tris-HCl (tris(hydroxyméthyl) aminométhane) pH 6.8, 2% SDS, 10 % glycerol, 0.01 % bromophenol blue). Twenty-five µg of protein extract was run on Sodium Dodecyl Sulfate Polyacrylamide Gel Electrophoresis (SDS-PAGE) in 10% acrylamide gel (10 % acrylamide, 70 µM TEMED, 0.0004 % ammonium persulfate, 0.376 M Tris-HCl pH 6.3, 0.001 % SDS). The gel was transferred to a Polyvinylidene difluoride (PVDF) membrane (90 min, 0.16 mA), the membrane was then incubated for 1 h in a blocking solution composed of 0.5 % semi-skimmed milk powder in TBST (Tris-buffered saline 20 mM, 0.1 % Tween 20) and then incubated with the anti-glutathione (1:1000) (Invitrogen) primary antibody solution ((milk 0.5 % TBST) at 4 °C overnight. After washing with TBST (3x5 min), the membrane was incubated for 1h with a solution containing a secondary goat-HRP -anti-rabbit (1:10 000) (Biorad) (milk 0.5 % TBST). After washing with TBST (3x5 min), the revelation was carried out by incubating the membrane using the substrate HRP immobilon Western kit. The intensity of each line was quantified using ImageJ and the mean +/- SD of 3 replicates was shown.

Measurements of the GST activity were performed on total proteins extracted as described above and the activity was detected using the GST substrate 1-chloro-2,4-dinitrobenzene (CDNB, Sigma-Aldrich). The GST-mediated reaction of CDNB with glutathione

produces a conjugate that is measured by absorbance at 340 nm. Typically, 20 µl protein extracts were incubated in 1 ml containing 0.1 M phosphate buffer pH 7, 0.5 mM CDNB and 2 mM GSH.

Detection of reactive oxygen species

Detection of ROS was performed as previously described (Mhamdi *et al.*, 2010). Staining was done at room temperature on 7-day-old Col-0 plants. For the detection of superoxides, plants were vacuum infiltrated in the Nitro Blue Tetrazolium (NBT) staining medium (10 mM phosphate buffer pH 7.5, 10 mM Na azide, 1 tablet of NBT (10 mg Sigma)). For the detection of H_2O_2, plants were vacuum infiltrated in 5 mM 3, 3'- Diaminobenzidine (DAB) at pH 3.8. For both stainings, plants were then incubated in the same medium until coloration was observed. Chlorophyll was removed in 95% ethanol and pictures were taken.

Glutathione measurements

The total glutathione content of 10-day-old seedlings was determined using the recycling enzymatic assay (Rahman *et al.*, 2006). The method consists of the reduction of GSSG to GSH by the glutathione reductase in presence of NADPH. GSH levels are determined by its oxidation by 5,5'-dithio-bis (2-nitrobenzoic acid) (DTNB, Sigma-Aldrich), which produces 5'-thio-2-nitrobenzoic acid (TNB), a yellow compound measurable at 412 nm (Rahman *et al.*, 2006). Briefly, 100 mg of fresh plant material was ground in liquid nitrogen and resuspended in 0.5 ml of 0.1 M Na phosphate buffer, pH 7.6, and 5 mM EDTA. After microcentrifugation (10 min, 9000 g), total glutathione in 0.1 ml of the supernatant was measured by spectrophotometry in a 1 ml mixture containing 6 mM DTNB, 3 mM NADPH, and 2 U of glutathione reductase from *Saccharomyces cerevisiae* (Sigma-Aldrich). Glutathione-dependent reduction of DTNB was monitored at 412 nm. Total glutathione

levels were calculated using the equation of the linear regression obtained from a standard GSH curve. GSSG was determined in the same extracts after derivatization of reduced GSH. Derivatization of 100 µl of plant extract was performed in 0.5 ml of 0.5 M K phosphate buffer, pH 7.6, in the presence of 0.8 % (v/v) of 2-vinylpyridine (Sigma-Aldrich) during 1 h at room temperature. After extraction of the GSH-conjugated 2-vinylpyridine with 1 volume of diethylether, GSSG content was measured by spectrophotometry as described for total glutathione.

Confocal Laser-Scanning Microscopy of roGFP2 and PlaCCI observations

Confocal microscopic observations were carried out using the Axio observer Z1 microscope with the LSM 700 scanning module and the ZEN 2010 software (Zeiss). Excitation of roGFP2 was performed at 488 and 405 nm and a bandpass (BP 490-555 nm) emission filter was used to collect the roGFP2 signal. The signal recorded using a BP 420-480 nm emission filter during excitation at 405 nm was used for background subtraction. Pictures analysis and quantifications of the roGFP2 redox ratios were performed using the Redox Ratio Analysis software developed by Pr. Mark Fricker (University of Oxford, UK) (Fricker, 2016). For cell cycle analysis with the Plant Cell Cycle Indicator (PlaCCI) line, plants were grown for 7 days at 20°C and then subjected to high temperature for 2.5 h. Live imaging of the cell cycle progression was recorded in root tips using confocal microscopy. Excitation of CDT1a-CFP, H3.1-mCherry and CYCB1;1-YFP were performed at 405nm, 555nm and 488nm respectively.

Statistical analyses

Data analysis was conducted in RStudio (RStudio Team (2020), http://www.rstudio.com/), statistical analysis was performed using the package Rstatix and figures were produced using the package ggplot2 (Wickham, 2016). For TMHT assays, means from at least 3 independent replicates were compared with one-way ANOVA followed by a post hoc Tukey's honestly significant difference test (HSD) *(** P ≤ 0.01, ** P ≤ 0.001, *** P ≤ 0.0001, *ns* P > 0.05*)*. For thermomorphogenesis assays, a Kruskal-Wallis ANOVA (non-parametric) followed by a Pairwise Wilcoxon test (P-value adjustment method: holm) (* P ≤ 0.01, ** P ≤ 0.001, *** P ≤ 0.0001, *ns* P > 0.05) was used. For the experiments concerning redox ratio, glutathione content, protein S-glutathionylation, cell frequency and gene expression, a pairwise two-tailed Student's t-test (* or $^{\#}$ P ≤ 0.05, ** or $^{\#\#}$ P ≤ 0.01, *** or $^{\#\#\#}$ P ≤ 0.001, ns P > 0.05) was used.

Results

High temperature regimes induce cytosol and nuclear oxidation

To explore the impact of high temperatures on the cytosolic glutathione redox potential (E_{GSH}) in cotyledons and root tip, we used as a proxy wild-type plant expressing the GRX1-roGFP2 in the cytosol (Gutscher et al., 2008). Calibration was made against 100 mM H_2O_2 and 10 mM DTT to fully oxidize or reduce the sensor, respectively (Fig. 1A-E). At 20°C, the fluorescence ratio was close to the ratio measured after DTT treatment, suggesting that under unstressed conditions the redox sensor is almost fully reduced. When the temperature is shifted to 27°C, the 405/488 nm ratio does not change significantly in

cotyledons and root tips (Fig. 1A and B). However, a stronger heat treatment at 37°C triggers fast oxidation of the roGFP2 in cotyledons, reaching almost full oxidation after 30 minutes of treatments (Fig. 1C). The ratio also increases in the root tip from 15 min to 60 min at 37°C but does not reach full oxidation (Fig. 1D). Therefore, we concluded that a moderate increase in temperature (20°C to 27°C) has only a mild impact on the cytosolic glutathione redox potential, but that an intense temperature increase (20°C to 37°C) profoundly changes the cytosolic E_{GSH}.

The GRX1-roGFP2 constructs show localization in the nucleus because the fusion protein can diffuse through the nuclear pores (Meyer et al., 2007). This enables us to study the effect of high temperatures on the E_{GSH} in the nuclear compartments (Babbar et al., 2021). When measuring the roGFP2 redox ratio by focusing our analysis on nuclei (Fig. 1F), we observed a progressive oxidation upon heat stress occurring after 10 minutes, which is significantly faster than in the cytosol (Fig. 1F). Later on, after 60 minutes of treatment, both nuclear and cytosolic compartments reach the same ratio, corresponding to a fully oxidized roGFP2. However, a 27°C treatment does not significantly change the 405/488 nm ratio in nuclei, as in the cytosol (Fig. 1F). Therefore, we conclude that the 37°C high temperature regime has a marked effect on the glutathione redox potential both in the cytosol and the nucleus, which is transiently faster in the nucleus.

Long-term effect of high temperatures on the glutathione redox state

As high temperatures conditions are generally lasting for several days, we studied the impact of high temperature regimes on the glutathione redox state in a longer term. Therefore, we quantified the pools of glutathione in plants subjected to high temperatures for 3 days (Fig. 2). Glutathione levels were monitored in 10-day-old plants subjected to the

same high temperature regimes of 27°C or 37°C. Both regimes led to a marked decrease (-35% and -50% at 27°C and 37°C, respectively) of the total extractible glutathione within the six first hours of the treatment. However, the decrease was more pronounced at 37°C than at 27°C, dropping within one hour while progressively decreasing after 2 hours at 27°C (Fig. 2A-B). Surprisingly, oxidized glutathione (GSSG) does not accumulate at much higher levels during heat treatments than in untreated plants (T0). Therefore, the GSH/(GSH+GSSG) is not profoundly modified during heat treatment, the most pronounced change in the GSH/(GSH+GSSG) ratio being observed after 1 hour of treatment at 37°C (from 87% to 73%) (Fig. 2B). Interestingly, at both temperatures, the glutathione levels increased after 24 hours of treatment, to reach about the same level as untreated plants after 3 days. Therefore, we conclude that both high temperature regimes affect the reduced glutathione level rather than the oxidized glutathione and that the glutathione pool is progressively restored after 3 days of high temperature regimes (Fig. 2A-B).

We further explored the rationale for the decreased extractible glutathione during heat stress, and we thought that protein S-glutathionylation might constitute a major sink for GSH during heat stress. Therefore, we quantified S-glutathionylated proteins in protein extracts of heat-treated plants (Fig. 2C). While a mild change in the S-glutathionylated protein profile was found at 27°C, compared to 20°C growing plants, a progressive increase of S-glutathionylated proteins were found in 37°C-treated plants. This increase correlated with an increase in the global glutathione-S-transferase (GST) activity of these plants, suggesting that glutathione conjugation might also contribute to the variation of the extractible glutathione pool (Fig. 2D). However, the kinetics of S-glutathionylation and GST activity being maximal at 3 days do not correlate with the early decrease (1-6 h) of the glutathione pool, suggesting that those activities might not have a major contribution in this

process. Thus, further investigation should be undertaken to understand the fate of glutathione after high temperature treatments.

High temperature regime changes the $O_2^{\cdot-}/H_2O_2$ balance in the root

We next wished to evaluate the impact of high temperatures on ROS accumulation *in planta*. For that purpose, we stained high temperature-treated plants with diaminobenzidine (DAB) or nitrobluetetrazolium (NBT) which react with H_2O_2 and $O_2^{\cdot-}$ respectively. At 20°C, the highest DAB staining were found in the root, while NBT staining was also found in cotyledons (Supplementary Fig. S1A and D). No significant change was observed after 2 hours treatment at 27°C or 37°C in any plant tissues, suggesting both high temperature regimes do not generate massive $O_2^{\cdot-}$ and H_2O_2 in most plant tissues (Supplementary Fig. S1B-C and E-F). The same DAB and NBT staining patterns were observed This contrasts with ROS accumulation observed by Babbar et al., (2021), in plants subjected to a 1 hour 42°C treatment, in which accumulation of DAB and NBT stainings were observed in shoot. However, in the root tip, a marked change in the DAB and NBT staining was observed at 37°C (Supplementary Fig. S1G-L). At 20°C and 27°C, the highest DAB staining is found in the elongation zone, as NBT signal is the highest in the root tip, as previously shown (Dunand *et al.*, 2007; Tsukagoshi *et al.*, 2010) (Supplementary Fig. S1G-H and J-K). However, at 37°C, high DAB staining is found in the meristem, while NBT is lower, suggesting that high temperatures lead to a change in $O_2^{\cdot-}$/ H_2O_2 balance (Supplementary Fig. S1 I-L).

The balance between $O_2^{\cdot-}$ and H_2O_2 is associated with the transition from the distal meristematic zone, where $O_2^{\cdot-}$ is predominant, to the basal maturing zone, in which H_2O_2 predominates (Dunand *et al.*, 2007). As this gradient regulates the proper transition from cellular proliferation to differentiation (Tsukagoshi et al., 2010), we investigated whether the observed change in the $O_2^{\cdot-}/H_2O_2$ balance under high temperature is associated with cell proliferation arrest in the root tip. To this purpose, we used the fluorescent sensor Plant Cell Cycle Indicator (PlaCCI) expressing the CDT1a-CFP, H3.1-mCherry and CYCB1;1-YFP, that identify cell cycle phases (Desvoyes *et al.*, 2020). Plants grown at 20°C show constant percentage of G1 (blue cells), S + early G2 (red cells) and late G2 + M (yellow cells) when followed during 2.5 hours, indicating that cells are "normally" progressing through the cell cycle (Supplemental Figure S2A, C and E). Consistently, G2 cells are progressing to M and G1 (Supplemental Figure S2A, insets). However, plants subjected to 37°C show a progressive deviation of the G1, S + early G2 and late G2 distribution, with an accumulation of cells in late G2 (Supplemental Figure S2B, D and F). Moreover, we never observed G2 cells progressing to the M phase, suggesting that a 37°C treatment arrests cell cycle at the late G2 phase (Supplemental Figure S2B, insets).

Low glutathione impairs thermotolerance

As the steady-state level of extractible reduced glutathione is mostly affected under high temperatures, we studied the response to high temperatures of the *cadmiumsensitive2* (*cad2*), which contains a low level of glutathione due to impaired glutathione synthesis capacities (Howden et al., 1995; Cobbett et al., 1998). First, we measured the glutathione levels in the *cad2* mutant subjected to the same high temperature regimes as previously (Fig. 3A). In agreement with previous reports, the total extractible glutathione level is about

12% compared to wild-type plants (Bashandy et al., 2010). Total glutathione levels noticeably decrease after 6 hours of high temperature (both 27°C and 37°C) treatments, as compared to wild-type plants (Fig. 2A-B). However, after 72 hours treatments, as the glutathione level slightly increases at 27°C, it dramatically dropped at 37°C (Fig. 3A).

We also measured the glutathione redox state in the *cad2* mutant, using the GRX1-roGFP2 construct introgressed in *cad2* (Meyer et al., 2007). The roGFP2 redox ratio behaves similarly in both backgrounds upon DTT and H_2O_2 treatements (Fig. 3B). As previously described, the roGFP2 probe is already partially oxidized under standard temperature conditions, which is due to a lower glutathione redox potential (Fig. 3C-D, 20°C) (Meyer et al., 2007). As expected, the roGFP2 becomes fully oxidized in the *cad2* mutant after 37°C treatment (Fig. 3C). However, the oxidation kinetics is more rapid than in wild-type plants since the roGFP2 is almost fully oxidized within 15 minutes (Fig. 3C). Even more striking is the rapid full oxidation of the roGFP2 observed at 27°C in the *cad2* mutant, while the same treatment hardly affects the roGFP2 ratio in wild-type plants (Fig. 3D). Therefore, we conclude that the glutathione redox potential is more sensitive to high temperatures in the *cad2* mutant as in wild-type plants.

Next, we studied the response of the low glutathione mutants to the same high temperature regimes. A 37°C heat regime mimicking a heat wave is commonly called Thermotolerance to Moderate High Temperature (TMHT) (Yeh et al., 2012; Martins et al., 2020). Here, seeds are germinated at a standard temperature for 4 days before being transferred to 37°C for 5 further days. Plants are switched again to 20°C to let them recover from the stress. After 11 days of recovery, the viability of the plants was assessed by the recovery of shoot growth (Fig. 4A). About 80% of wild-type plants survived the TMHT

treatment while the survival rate in *cad2* plants was profoundly affected (Fig. 4B-C). To confirm this observation, we submitted another low glutathione mutant, *phytoalexin-deficient mutant* (*pad2*-1, Parisy et al., 2007), to the same treatment. The viability of *pad2-1* was as affected as *cad2* at 37°C (Fig. 4C). To further confirm that impaired glutathione level is responsible for the loss of plant survival rate under TMHT, we treated wild-type plants with increasing concentrations of the glutathione biosynthesis inhibitor buthionine sulfoximide (BSO). As BSO did not affect plant viability at 20°C, it led to a dose dependent inhibition of plant survival rate at 37°C, reaching an almost null value at 1 mM BSO, an effect as strong as the *hsfa1QK* mutation that we used as a positive control (Fig. 4C-D; Yeh et al., 2010). To study whether a perturbed glutathione redox state may also impact the response to TMHT, we subjected the cytosolic glutathione reductase mutant *gr1* to the same treatment (Marty et al., 2009). In contrast to glutathione deficient mutants, the survival rate of *gr1* was not perturbed (Fig. 4C), indicating that the glutathione level rather than the glutathione redox state impairs plant survival to TMHT.

As low glutathione might impact the activity of enzymes which use glutathione as a co-factor like glutaredoxins, we wished to evaluate whether *grx* mutants from our collection were impacted by TMHT. Thus, we subjected different cytosolic *grx* mutants to TMHT (Fig. 4C). None of the studied *grx* mutants was affected by TMHT, in contrast to the previously described *grxS17* knock-out mutants (Martins et al., 2020). As heat stress induces ROS accumulation, we also studied the behaviour of mutants affected in the ROS metabolism. The catalase2 (c*at2*) mutant inactivated in a major H_2O_2 catabolic enzyme was also affected by TMHT (Fig. 4C). We also monitored the thermotolerance of GSNO and NO accumulating mutants to TMHT. The GSNO reductase mutant *gsnor-1/hot5* was previously shown to be

intolerant to a 45°C heat treatment (Lee et al., 2008). Here, we found that the *gsnor-1* mutant is also intolerant to a 37°C TMHT treatment (Fig. 4C). Finally, we also found the NO accumulating mutant *nox1* to be highly sensitive to TMHT, as previously described at 45°C (Lee et al., 2008) (Fig. 4C).

Low glutathione impairs thermomorphogenesis

As we found that the glutathione steady-state levels are affected by a 27°C treatment (Fig. 2A), we also studied the behaviour of low glutathione mutants to a 27°C high temperature treatment applied for 7 days (Fig. 5A). As previously shown, this regime induces a thermomorphogenesis adaptation monitored by elongation of the hypocotyl (Fig. 5A). At 20°C, hypocotyl length of *cad2* and *pad2* mutants is like Col-0 (Fig. 5C). However, when subjected to 27°C, the hypocotyl elongation observed in wild-type plants is partially impaired in both *cad2* and *pad2*, suggesting that low glutathione impairs high temperature-induced hypocotyl elongation (Fig. 5C). In contrast, high temperature-dependent hypocotyl elongation was not affected in the cytosolic glutathione reductase mutant (*gr1*), suggesting that glutathione level rather than glutathione redox state is involved in thermomorphogenesis (Fig. 5C). As for TMHT, we also subjected *grx* mutants to the thermomorphogenesis regime. Interestingly, *grxc3* and *grxc4* mutants had significantly shorter hypocotyls than wild-type plants at 27°C while also very slightly shorter at 20°C, suggesting that these two GRXs might be involved in the low glutathione-dependent hypocotyl elongation phenotype (Fig. 5D).

Finally, we re-analyzed the hypocotyl elongation of two mutants impaired in master regulators of the thermomorphogenesis regulation (Jung et al., 2016; Legris et al., 2016; Gangappa and Kumar, 2017). As previously described, both mutants have contrasted

hypocotyl elongation phenotypes. While the *phytochrome b* (*phyb)* mutant has a long hypocotyl at both 20°C and 27°C, due to constitutively induced thermomorphogenesis, the *phytochrome-interacting factor 4 (pif4)* mutant fails to induce hypocotyl elongation at 27°C due to its impaired thermomorphogenesis pathway (Supplementary Fig. S3A and C). To study whether the lack of thermomorphogenesis of the *pif4* mutant also affects its thermotolerance, we subjected *pif4* to TMHT. The viability of the *pif4* mutant is not affected, indicating that the thermomorphogenesis pathway does not overlap with the tolerance to TMHT. However, the *phyb* mutant shows a low survival rate to TMHT, which can be due to his long hypocotyl phenotype (Supplementary Fig. S3B and D).

To examine if glutathione is involved in the *PHYB*/*PIF4*-dependent thermomorphogenesis regulation, we applied low concentrations (0.2 mM) of exogenous BSO on *pif4* and *phyb* mutants and measured hypocotyl length under 20°C or 27°C. Interestingly, BSO-treated *pif4* plants show a stronger reduction of hypocotyl elongation as untreated *pif4* at 27°C, suggesting that the glutathione effect on hypocotyl elongation is independent of the PIF4 thermomorphogenesis pathway (Supplementary Fig. S3E). On the contrary, the *phyb* long hypocotyl phenotype is exacerbated by BSO treatment (Supplementary Fig. S3F).

Low glutathione influences transcriptional response to high temperatures

Given the observed transient glutathione decrease in both cytosol and nuclear compartments in response to heat stress and that the response to heat is impaired in low glutathione mutants, we wished to explore the impact of both high temperature regimes on genome expression in both wild-type and the low glutathione mutant *cad2*. Therefore, we performed a wide transcriptomic analysis by RNA-seq. Wild-type and *cad2* plants were

treated in the same conditions as previously described (20°C, 27°C and 37°C) and samples from three biological repetitions were taken before and during temperature treatments, at times coinciding with the decrease (2 h) and during the recovery of glutathione level (24 h) (Fig. 2A-B). The reliability of the RNAseq analyses was assessed by PCA analyses (Supplementary Fig. S4) and differentially expressed genes (DEG) were selected with a 2-fold cutoff (Padj<0.01) (Supplementary Dataset 1). We first analyzed the impact of high temperatures on gene expression deviation in wild-type plants (Supplementary Fig. S5). As expected, a 37°C treatment has a much stronger effect on gene expression reprogramming than a 27°C treatment: 12189 (5600 upregulated, 6499 downregulated) and 891 (437 upregulated, 454 downregulated) genes whose expression is modified after stress, respectively. A large majority of differentially expressed genes (64% up-, 90% down-regulated) at 27°C treatment was common with 37°C treatments, indicating that both treatments trigger a common gene regulation signature (Supplementary Fig. S5C-D). Gene ontology (GO) analyses associate common responses with 'stimulus, stress and high temperature' responses (Supplementary Fig. S5B).

Then, we evaluated the impact of the *cad2* mutation on gene expression after heat stress (Fig. 6 and 7). At 27°C, we identified 387 genes that were differentially expressed upon high temperature treatment in both genotypes. Consistent with the temperature treatment imposed on the plants, the shared regulatory signatures were associated with heat response [GO categories: response to heat, temperature, stress] (Fig. 6B). We also observed contrasting regulatory responses between wild-type and *cad2* mutants. Heatmap analyses delineated misregulated genes in different clusters. Among them, several clusters correspond to genes that are misexpressed at 2h or 24h upon high temperature [GO

categories: response to abiotic stress and temperature stimulus, response to ROS] (Fig. 6C-D). Interestingly, among differentially expressed genes between wild-type and *cad2*, GO categories underline a differential response to oxidative stress (Fig. 6B). Taken together, these results show that in addition to common core regulatory signatures, the *cad2* mutant displays specific responses to elevated ambient temperature.

Comparison of the gene expression profiles between wild-type and *cad2* plants subjected to 37°C also shows a large panel of common differentially expressed genes in both genetic backgrounds (78% of differentially expressed genes), indicating that major heat stress response pathways are not perturbed in the *cad2* mutant (Fig. 7A-B). Among them, major heat stress response genes like *HSPs* (101, 90, 70, small HSPs), *HSF* transcription factors or known heat stress-induced antioxidant enzymes like *APX2*, show no, or mild modifications in transcripts accumulation in the mutant, (Supplementary Fig. S6). However, major differentially expressed clusters were also found to be specifically expressed in wild-type or *cad2* mutants (Fig. 7A). GO categories underline a differential response to developmental processes in wild-type and ion binding capacities in *cad2*, respectively (Fig. 7B).

To characterize whether glutathione metabolism genes are differentially regulated in the *cad2* mutant upon high temperature, we selected a panel of 165 genes encoding proteins involved in glutathione metabolism/catabolism or which use glutathione as substrate (Fig. 8A and Supplementary Table 1) and analyzed their expression upon both high temperature regimes. A heatmap shows that most of the genes have a common response to high temperature, indicating that these genes are not much impacted by the stress treatments at the transcriptional level. Core glutathione synthesis (*GSH1, GSH2*) and

reduction (*GR1*) genes show a mild but significant increase of the transcript numbers upon high temperature (Fig. 8B). Moreover, several genes encoding for glutathione-S-transferases (GSTs), show differential expression (Fig. 8B). Among them, different isoforms of plant specific *phi* (GSTF) and *tau* (GSTU) classes are glutathione-conjugating enzymes involved in different stress responses (Dixon and Edwards, 2010; Sylvestre-Gonon et al., 2020). These isoforms might have relevant functions upon heat stress.

Finally, to ascertain that the transcriptomic deviation we observed in *cad2* shows similar effects in another low glutathione mutant, we compared the *cad2* transcriptome with *pad2* under the same high temperature conditions performed for 2 hours (Supplementary Dataset 2). Multidimentional scaling (MDS) plot of all RNAseq samples showed that both *cad2* and *pad2* genotypes cluster well together, and are both distinct from Col-0 samples, indicating that both mutants show a similar gene expression deviation compared to Col-0 (Supplementary Fig. S7). We also verified that several DEG genes behave similarly between *cad2* and *pad2*, validating that the observed transcriptomic deviation we observed in the *cad2* mutant upon high temperatures is similarly occurring in an independent low glutathione mutant *pad2* (Supplementary Fig. S8).

All in all, the genome-wide gene expression analyses indicate that, while low glutathione mutants share the most common response to heat temperature with wild-type plants, it also shows deviations in the response which might participate to the sensitivity of the *cad2* and *pad2* mutants to both high temperature regimes.

Discussion

High temperature leads to cytosolic and nuclear oxidation

In this work, we investigated the contribution of glutathione in the cellular responses to two contrasted high-temperature regimes, 27°C inducing thermomorphogenesis and 37°C, triggering heat stress responses. First, we studied the impact of high temperatures on the dynamics of glutathione redox state. We show that, while a 27°C treatment hardly impacts the redox state of the roGFP2, at least during the first hour after the treatment, a 37°C treatment rapidly induces a full roGFP2 oxidation (Fig. 1). Indeed, the full oxidation of the probe brings it outside its measuring range of about -310 to -250 mV, which limits its usability to measure the actual E_{GSH} value. Therefore, we can only estimate that the 37°C temperature condition decreases the glutathione redox potential to > 250 mV. The effect of high temperature on E_{GSH} measurement should be more accurately estimated by using less reducing probe variants like the roGFP2-iL (Aller et al., 2013; Ugaldo et al., 2022). In a previous report, Babbar et al. (2021) have also observed a marked change in the glutathione redox potential (about -330 mV to -250 mV) of the cytosol and nuclei of epidermal and stomatal guard cells after a 1h heat stress at 42°C. Consistently, our data support similar oxidation of the roGFP2 in the nuclear compartment which seems to occur even faster as the cytosol at 37°C (Fig. 1F). Such a slightly faster nuclear roGFP2 oxidation kinetic should be further confirmed by other ways but could provide from a lower nuclear glutathione reduction capacity or a slight difference in the glutathione cytosolic/nuclear fluxes during heat stress (Diaz Vivancos *et al.*, 2010; Delorme-Hinoux *et al.*, 2016).

As a sensor of the redox state of glutathione, roGFP2 oxidation is generally associated with the accumulation of oxidized glutathione, for example in glutathione reductases

mutants or plants accumulating high H_2O_2 levels (Marty *et al.*, 2009, 2019). However, we did not observe a massive accumulation of oxidized glutathione after the raise of temperature but rather a marked decrease of the total glutathione pool (Fig. 2). Such a decrease of the glutathione poll was also previously reported in cucumber subjected to 35°C heat treatments (Ding et al., 2016). Although this decrease leads to a mild change of the GSSG/GSH ratio during the first hours after the treatments, such a slight modification of the GSSG/GSH redox equilibrium hardly explains the almost full oxidation of the roGFP2. Moreover, our *in situ* ROS detection did not reveal massive ROS accumulation in leaves upon heat stress at 37°C, indicating that ROS accumulation is unlikely to be responsible for the roGFP2 oxidation (Supplementary Fig. S1). In another hand, roGFP2 is also oxidized under conditions of limited amount of the glutathione pool, like under pharmacological treatments with glutathione biosynthesis inhibitors (BSO or CDNB) or in low glutathione genetic mutants (*cad2, pad2, rml1*) (Meyer *et al.*, 2007; Maughan et al., 2010; Aller et al., 2013). We accordingly found the roGFP2 partially oxidized at 20°C in the *cad2* mutant (Fig. 3B). Moreover, the partial depletion of the glutathione pool in *cad2* somehow intensify the effect of high temperature on roGFP2 oxidation (Fig. 3). Even at 27°C, the roGFP2 is rapidly fully oxidized, as it was hardly the case in the wild-type background (Fig. 1). This might be attributed to the lower redox buffering capacity or to a weaker antioxidant capacity of this low glutathione mutant upon high temperature.

The transient decrease of the glutathione pool upon high temperature treatments is intriguing (Fig. 2A-B). The significance and the mechanism behind this observation will have to be further investigated. A hypothesis we tested to understand the fate of glutathione was conjugation of GSH to acceptor molecules like protein S-glutathionylation. However, the kinetics of our protein S-glutathionylation assays do not support a major contribution of this

pathway (Fig. 2C). Nevertheless, at least at 37°C, the progressive accumulation of S-glutathionylated proteins might protect them against high temperature injuries. It would be of future interest to identify the nature of these proteins. Increased GST activity (Fig. 2D) might also contribute to thermotolerance, potentially through glutathione conjugation to metabolites or other compounds (Dixon and Edwards, 2010; Sylvestre-Gonon et al., 2020). Specific *GSTF* and *GSTU* isoforms found differentially expressed in our RNAseq analyses, might be involved in this response (Supplementary Table 1 and Dataset 1). Different types of enzymes are involved in glutathione catabolism: carboxypeptidases, phytochelatin synthases, gamma-glutamyl transpeptidases (GGT), gamma-glutamyl cyclotransferases (GGCT) (Meister, 1988; Ohkama-Ohtsu et al., 2007; Blum *et al.*, 2007, 2010; Meyer *et al.*, 2012; Joshi et al., 2019). Among them, the cytosolic GGCT2;1 has been shown to mobilize L-cysteine from glutathione for *de novo* L-cysteine synthesis during sulfur starvation (Joshi et al., 2019). The contribution of these enzymes in the high temperature-dependent glutathione decay will have to be further investigated. Our biochemical glutathione measurements also point to the capacity of plants to recover a steady state level of glutathione after three days of continuous high temperature treatment which likely participates in the adaptation of the plant to high temperature (Fig. 2). The level of glutathione has been previously shown to correlate with the adaptation of plants to temperature stress, which is associated with an adjustment of the glutathione metabolism and antioxidant activities of the plant (Li et al., 2013; Nahar et al., 2015; Ding et al., 2016). While we do observe a mild increase of the glutathione biosynthesis gene (*GSH1, GSH2*) expression during the recovery period (Fig. 8), we may also assume that increased GSH1 or GSH2 enzyme activity might be responsible for the readjustment of the glutathione steady-state level after a few days of these treatments.

Adjusted glutathione pool is required for tolerance to high temperature regimes

The requirement of a "high" glutathione steady-state level to allow plant tolerance to high temperature is evidenced by the sensitivity of the glutathione deficient mutants (*cad2, pad2*) and BSO-treated plants, to high temperature regimes. Somehow supporting the minor change in the glutathione redox state upon high temperature, the *gr1* mutant inactivated in the cytosolic/nuclear glutathione reductase is hardly affected by high temperature (Fig. 4 and 5). Nevertheless, the role of the thioredoxin pathways as a backup for glutathione reduction has also to be considered in the context of the plant response to high temperatures (Marty *et al.*, 2009, 2019).

The fact that the two high temperature regimes we studied here induce different plant responses implies that glutathione can be involved in both pathways (Fig. 4, 5). Indeed, thermomorphogenesis induction involves many regulatory pathways which might be under redox control. Still, our data suggest that the PHYB/PIF4 module is likely not a direct target of a glutathione-dependent regulation (Supplementary Fig. S3), other actors involved in the thermomorphogenesis pathway might be glutathione regulated. Among them, hormones like auxin, brassinosteroids and GA are clearly involved in thermomorphogenesis (Casal and Balasubramanian 2019; Gray *et al.*, 1998; Sun *et al.*, 2012). While our RNAseq analysis fails to identify clear GO categories of thermomorphogenesis genes among the differentially expressed genes in the *cad2* mutant, we do observe some differences in individual genes like *PIF4* or some auxin metabolism genes (Supplementary Fig. S6). Moreover, clear connections between glutathione/glutaredoxins and auxin and brassinosteroids metabolism have been previously described in other plant development aspects (Bashandy *et al.*, 2010; Schnaubelt *et al.*, 2015; Bender *et al.*, 2015; Trujillo-Hernandez *et al.*, 2020). The observation that some glutaredoxins mutants also harbour hypocotyl elongation defects

gives clues for future research (Fig. 5). Thus, the contribution of these actors to the thermomorphogenesis regulation will have to be further investigated, for example by further exploring the genetic crosstalks between glutathione and thermomorphogenesis mutants. Similarly, we have shown that plant tolerance to the TMHT regime (37°C) requires an appropriate pool of glutathione, as both *cad2*, *pad2* and BSO-treated plants are unable to survive the treatment (Fig. 5). In contrast, an affected glutathione redox state in the *gr1* seems not a major factor for the survival with respect to alternative reduction pathway which might occur (Marty *et al.*, 2009).

High temperature transcriptional reprogramming is partially glutathione-dependant

The transient variation of the glutathione pool after high temperature exposition (Fig 2A-B) might also play roles to signal stress and induce transcriptomic responses. The rapid roGFP2 oxidation we found in the nucleus under high temperature could also support the role of glutathione in gene expression regulation upon heat stress (Fig. 1F). Glutathione-dependent transcriptomic signatures have been previously documented in low glutathione mutants under stress conditions (Ball *et al.*, 2004; Assmann, 2013; Schnaubelt *et al.*, 2015; Willems et al., 2016). And glutathione is also known to induce heat stress responsive genes through activation of specific transcription factors (Kumar and Chattopadhyay, 2018). Indeed, our genome-wide gene expression analyses identified substantial deviations in gene expression reprogramming in the *cad2* mutant (Fig. 6-8), suggesting that the transcriptional responses to high temperatures are partially altered in the mutant. Although major high temperature response pathways (e.g. HSPs) were found to be induced as in the wild-type, several clusters of genes appeared to be differentially expressed in the *cad2* mutant (Fig. 6 and 7). Among the GO categories identified, we can assume that some “high

temperature/stress response" pathways are misexpressed. Nevertheless, this does not mean that this transcriptional deviation is responsible for the thermotolerance defect of the *cad2* mutant. For example, the observed decrease in the expression of *PIF4* in the mutant subjected to 27°C can be the consequence of impaired thermomorphogenesis, rather than its cause (Supplementary Fig. S6). How glutathione is acting in the thermomorphogenesis pathways will have to be further studied.

When focusing our RNAseq analyses on glutathione-dependent genes, it is interesting to notice that many GSTs have differential expression levels after high temperature treatments. This is more pronounced under the 37°C regime, for which protein S-glutathionylation was found (Fig. 2C), suggesting that proteins involved in glutathione conjugation might be particularly mobilized. In contrast, a batch of glutaredoxins, which generally act in protein S-deglutathionylation seems downregulated upon heat stress. However, no high temperature sensitivity was noticed in most of the glutaredoxin mutants we analyzed. This might be due to redundancy between members of the large glutaredoxins family (Riondet *et al.*, 2012). However, an impaired thermotolerance of the *grxS17* was previously reported (Cheng *et al.*, 2011; Knuesting *et al.*, 2015; Martins *et al.*, 2020). While at 27°C, the *grxS17* mutation was suggested to impair auxin signalling (Cheng *et al.*, 2011), the 35°C treatment was also suggested to induce holdase activities of GRXS17 (Martins *et al.*, 2020). Whether a lower glutathione level would limit GRXS17 thermotolerance activities should be further investigated.

Conclusions

In this study, we describe the dynamics of redox changes occurring under two different high temperature regimes. Using the GRX1-roGFP2 redox sensor, we show that high temperature induces oxidation of the cytosolic and nuclear compartments, which is mainly due to a decrease in the total glutathione level. However, plants can restore a steady state level after at least one day of treatment, such adaptation likely being required both for the temperature-dependent developmental (thermomorphogenesis) and tolerance capacities of the plant. Further investigations are required to decipher the downstream actors of the glutathione-dependent adaptation to high temperature, but our genome-wide transcriptomic data suggest that genome reprogramming likely plays a key role in this response. Thus, our work aiming to better understanding the role of the glutathione pathway in regulating plant responses to high temperatures might contribute to heat stress improvement in Arabidopsis and possibly other crops.

Acknowledgments

We are grateful to Bénédicte Desvoyes and Crisanto Gutierrez for providing us PlaCCI seeds, and to Michèle Laudié and Margot Doberva from the Bio-Environment platform (University of Perpignan Via Domitia) for technical support in library preparation and sequencing.

Author Contributions

Conceptualization, AD, CR and JPR.; research performing, AD, AW, LB and CR; RNA-seq raw data analysis, NP and FP; writing, review and editing, AD and JPR; All authors have read and agree with the present version of the manuscript.

Conflict of interest

The authors declare that they have no conflict of interest.

Funding

This work was funded by the Centre National de la Recherche Scientifique, by the Agence Nationale de la Recherche (grant nos. ANR-REPHARE 19–CE12–0027 and ANR-RoxRNase 20-CE12-0025). This project was funded through Labex AGRO (under I-Site Muse framework) coordinated by the Agropolis Fondation (grant no. Flagship Project 1802-002 - CalClim). This study is set within the framework of the Laboratoires d'Excellence TULIP (ANR-10-LABX-41) and the Ecole Universitaire de Recherche (EUR) TULIP-GS (ANR-18-EUR-0019). AD is supported by a Ph.D. grant from the Université de Perpignan Via Domitia (Ecole Doctorale Energie et Environnement ED305).

Data Availability

All data supporting the findings of this study are available within the paper and within its supplementary materials published online. RNAseq data are openly available at the following link: www.ebi.ac.uk/ena/browser/view/PRJEB52103

References

Aller I, Rouhier N, Meyer AJ. 2013. Development of roGFP2-derived redox probes for measurement of the glutathione redox potential in the cytosol of severely glutathione-deficient rml1 seedlings. Frontiers in Plant Science **4**, 506. doi: 10.3389/fpls.2013.00506.

Anders S, Pyl PT, Huber W. 2015. HTSeq--a Python framework to work with high-throughput sequencing data. Bioinformatics **31**, 166–169.

Assmann SM. 2013. Natural Variation in Abiotic Stress and Climate Change Responses in Arabidopsis: Implications for Twenty-First-Century Agriculture. International Journal of Plant Sciences **174**, 3–26.

Babbar R, Karpinska B, Grover A, Foyer CH. 2021. Heat-Induced Oxidation of the Nuclei and Cytosol. Frontiers in Plant Science **11**, 617779.

Bailey-Serres J, Parker JE, Ainsworth, EA, Oldroyd GED, Schroeder JI. 2019. Genetic strategies for improving crop yields. Nature **575**, 109-118.

Ball L, Accotto G-P, Bechtold U, *et al.* 2004. Evidence for a direct link between glutathione biosynthesis and stress defense gene expression in Arabidopsis. The Plant Cell **16**, 2448–2462.

Bashandy T, Guilleminot J, Vernoux T, Caparros-Ruiz D, Ljung K, Meyer Y, Reichheld J-P. 2010. Interplay between the NADP-linked thioredoxin and glutathione systems in *Arabidopsis* auxin signaling. The Plant Cell **22**, 376–391.

Bender KW, Wang X, Cheng GB, Kim HS, Zielinski RE, Huber SC. 2015. Glutaredoxin AtGRXC2 catalyses inhibitory glutathionylation of Arabidopsis BRI1-associated receptor-like kinase 1 (BAK1) in vitro. The Biochemical journal **467**, 399–413.

Blair EJ, Bonnot T, Hummel M, Hay E, Marzolino JM, Quijada IA, Nagel DH. 2019. Contribution of time of day and the circadian clock to the heat stress responsive transcriptome in Arabidopsis. Scientific Reports **9**, 4814.

Blum R, Beck A, Korte A, Stengel A, Letzel T, Lendzian K, Grill E. 2007. Function of phytochelatin synthase in catabolism of glutathione-conjugates. The Plant Journal **49**, 740–749.

Blum R, Meyer KC, Wunschmann J, Lendzian KJ, Grill E. 2010. Cytosolic Action of Phytochelatin Synthase. Plant Physiology **153**, 159–169.

Bolger AM, Lohse M, Usadel B. 2014. Trimmomatic: a flexible trimmer for Illumina sequence data. Bioinformatics **30**, 2114–2120.

Casal JJ, Balasubramanian S. 2019. Thermomorphogenesis. Annual Review of Plant Biology **70**, 321–346.

Cheng N-H, Liu J-Z, Liu X, *et al.* 2011. Arabidopsis monothiol glutaredoxin, AtGRXS17, is critical for temperature-dependent postembryonic growth and development via modulating auxin response. The Journal of Biological Chemistry **286**, 20398–20406.

Choudhury FK, Rivero RM, Blumwald E, Mittler R. 2017. Reactive oxygen species, abiotic stress and stress combination. The Plant Journal **90**, 856–867.

Cobbett CS, May MJ, Howden R, Rolls B. 1998. The glutathione-deficient, cadmium-sensitive mutant, cad2-1, of Arabidopsis thaliana is deficient in gamma-glutamylcysteine synthetase. The Plant Journal **16**, 73–78.

Considine MJ, Foyer CH. 2014. Redox Regulation of Plant Development. Antioxidants & Redox Signaling **21**, 1305-1326.

Delorme-Hinoux V, Bangash SAK, Meyer AJ, Reichheld JP. 2016. Nuclear thiol redox systems in plants. Plant Science **243**, 84–95.

Desvoyes B, Arana-Echarri A, Barea MD, Gutierrez C. 2020. A comprehensive fluorescent sensor for spatiotemporal cell cycle analysis in Arabidopsis. Nature Plants **6**, 1330–1334.

Diaz Vivancos P, Wolff T, Markovic J, Pallardó FV, Foyer CH. 2010. A nuclear glutathione cycle within the cell cycle. The Biochemical Journal **431**, 169–178.

Ding et al., Jiang Y, He L, Zhou Q, Yu J, Hui D, Huang D. 2016. Exogenous glutathione improves high root-zone temperature tolerance by modulating photosynthesis, antioxidant and osmolytes systems in cucumber seedlings. Scientific Reports **6**, 35424. doi: 10.1038/srep35424.

Dixon DP and Edwards R. 2010. Glutathione transferases. Arabidopsis book **8**, e0131. Doi 10.1199/tab.0131.

Dunand C, Crèvecoeur M, Penel C. 2007. Distribution of superoxide and hydrogen peroxide in Arabidopsis root and their influence on root development: possible interaction with peroxidases. The New Phytologist **174**, 332–341.

Foyer CH, Noctor G. 2011. Ascorbate and Glutathione: The Heart of the Redox Hub. Plant Physiology **155**, 2–18.

Fricker, MD. 2016. Quantitative Redox Imaging Software. Antioxidants & Redox Signaling **24**, 752-62.

Gangappa SN, Kumar SV. 2017. DET1 and HY5 Control PIF4-Mediated Thermosensory Elongation Growth through Distinct Mechanisms. Cell Reports **18**, 344–351.

Giesguth M, Sahm A, Simon S, Dietz KJ. 2015. Redox dependent translocation of the heat shock transcription factor AtHSFA8 from the cytosol to the nucleus in Arabidopsis thaliana. FEBS Letters **589**, 718-725.

Gray WM, Ostin A, Sandberg G, Romano CP, Estelle M. 1998. High temperature promotes auxin-mediated hypocotyl elongation in Arabidopsis. Proceedings of the National Academy of Sciences of the United States of America **95**, 7197–7202.

Gutscher M, Pauleau A-L, Marty L, Brach T, Wabnitz GH, Samstag Y, Meyer AJ, Dick TP. 2008. Real-time imaging of the intracellular glutathione redox potential. Nature Methods **5**, 553–559.

Howden R, Andersen CR, Goldsbrough PB, Cobbett CS. 1995. A cadmium-sensitive, glutathione-deficient mutant of Arabidopsis thaliana. Plant Physiology **107**, 1067–73.

IPCC, 2021: *Climate Change 2021: The Physical Science Basis. Contribution of Working Group I to the Sixth Assessment Report of the Intergovernmental Panel on Climate Change* [Masson-Delmotte, V., P.

Zhai, A. Pirani, S.L. Connors, C. Péan, S. Berger, N. Caud, Y. Chen, L. Goldfarb, M.I. Gomis, M. Huang, K. Leitzell, E. Lonnoy, J.B.R. Matthews, T.K. Maycock, T. Waterfield, O. Yelekçi, R. Yu, and B. Zhou (eds.)]. Cambridge University Press, Cambridge, United Kingdom and New York, NY, USA, In press, doi:10.1017/9781009157896.

Jacob P, Hirt H, Bendahmane A. 2017. The heat-shock protein/chaperone network and multiple stress resistance. Plant Biotechnology Journal **15**, 405–414.

Joshi NC, Meyer AJ, Bangash SAK, Zheng ZL, Leustek T. 2019. Arabidopsis γ-glutamylcyclotransferase affects glutathione content and root system architecture during sulfur starvation. New Phytologist **221**, 1387-1397.

Jung J-H, Domijan M, Klose C, *et al.* 2016. Phytochromes function as thermosensors in Arabidopsis. Science **354**, 886–889.

Kim D, Langmead B, Salzberg SL. 2015. HISAT: a fast spliced aligner with low memory requirements. Nature Methods **12**, 357–360.

Knuesting J, Riondet C, Maria C, *et al.* 2015. Arabidopsis Glutaredoxin S17 and Its Partner, the Nuclear Factor Y Subunit C11/Negative Cofactor 2α, Contribute to Maintenance of the Shoot Apical Meristem under Long-Day Photoperiod. Plant Physiology **167**, 1643–1658.

Koini MA, Alvey L, Allen T, Tilley CA, Harberd NP, Whitelam GC, Franklin KA. 2009. High temperature-mediated adaptations in plant architecture require the bHLH transcription factor PIF4. Current biology **19**, 408–413.

Kumar D, Chattopadhyay S. 2018. Glutathione modulates the expression of heat shock proteins via the transcription factors BZIP10 and MYB21 in Arabidopsis. Journal of experimental botany **69**, 3729-3743.

Larkindale J, Hall JD, Knight MR, Vierling E. 2005. Heat stress phenotypes of Arabidopsis mutants implicate multiple signaling pathways in the acquisition of thermotolerance. Plant Physiology **138**, 882-97.

Lee U, Wie C, Fernandez BO, Feelisch M, Vierling E. 2008. Modulation of nitrosative stress by S-nitrosoglutathione reductase is critical for thermotolerance and plant growth in *Arabidopsis*. The Plant Cell **20**, 786–802.

Legris M, Klose C, Burgie ES, Rojas CCR, Neme M, Hiltbrunner A, Wigge PA, Schäfer E, Vierstra RD, Casal JJ. 2016. Phytochrome B integrates light and temperature signals in Arabidopsis. Science **354**, 897–900.

Li H, Handsaker B, Wysoker A, Fennell T, Ruan J, Homer N, Marth G, Abecasis G, Durbin R, 1000 Genome Project Data Processing Subgroup. 2009. The Sequence Alignment/Map format and SAMtools. Bioinformatics **25**, 2078–2079.

Li H, Wang XM, Chen L, Ahammed GJ, Xia XJ, Shi K, Considine MJ, Yu JQ, Zhou YH. 2013. Growth temperature-induced changes in biomass accumulation, photosynthesis and glutathione redox homeostasis as influenced by hydrogen peroxide in cucumber. Plant Physiology and Biochemistry **71**, 1-10.

Liu HC, Liao, HT, Charng YY. 2011. The role of class A1 heat shock factors (HSFA1s) in response to heat and other stresses in Arabidopsis. Plant, Cell and Environment **34**, 738-751.

Liu B, Asseng S, Liu L, Tang L, Cao W, Zhu Y. 2016. Testing the responses of four wheat crop models to heat stress at anthesis and grain filling. Global Change Biology **22**, 1890–1903.

Love MI, Huber W, Anders S. 2014. Moderated estimation of fold change and dispersion for RNA-seq data with DESeq2. Genome Biology **15**, 550.

Martins L, Knuesting J, Bariat L, *et al.* 2020. Redox modification of the Fe-S glutaredoxin GRXS17 activates holdase activity and protects plants from heat stress. Plant Physiology, **184**, 676-692.

Martins L, Trujillo-Hernandez JA, Reichheld J-P. 2018. Thiol Based Redox Signaling in Plant Nucleus. Frontiers in Plant Science **9**, 705.

Marty L, Bausewein D, Müller C, *et al.* 2019. Arabidopsis glutathione reductase 2 is indispensable in plastids, while mitochondrial glutathione is safeguarded by additional reduction and transport systems. New Phytologist **224**, 1569–1584.

Marty L, Siala W, Schwarzländer M, Fricker MD, Wirtz M, Sweetlove LJ, Meyer Y, Meyer AJ, Reichheld J-P, Hell R. 2009. The NADPH-dependent thioredoxin system constitutes a functional backup for cytosolic glutathione reductase in Arabidopsis. Proceedings of the National Academy of Sciences of the United States of America **106**, 9109–9114.

Maughan SC, Pasternak M, Cairns N, *et al.* 2010. Plant homologs of the Plasmodium falciparum chloroquine-resistance transporter, PfCRT, are required for glutathione homeostasis and stress responses. Proceedings of the National Academy of Sciences of the United States of America **107**, 2331-6.

Meister A. 1988. Glutathione metabolism and its selective modification. The Journal of Biological Chemistry **263**, 17205–17208.

Merret R, Descombin J, Juan YT, Favory JJ, Carpentier MC, Chaparro C, Charng YY, Deragon JM, Bousquet-Antonelli C. 2013. XRN4 and LARP1 are required for a heat-triggered mRNA decay pathway involved in plant acclimation and survival during thermal stress. Cell Reports **5**, 1279-93.

Meyer Y, Belin C, Delorme-Hinoux V, Reichheld J-P, Riondet C. 2012. Thioredoxin and Glutaredoxin Systems in Plants: Molecular Mechanisms, Crosstalks, and Functional Significance. Antioxidants & Redox Signaling **17**, 1124–1160.

Meyer AJ, Brach T, Marty L, Kreye S, Rouhier N, Jacquot J-P, Hell R. 2007. Redox-sensitive GFP in Arabidopsis thaliana is a quantitative biosensor for the redox potential of the cellular glutathione redox buffer. The Plant Journal **52**, 973–986.

Mhamdi A, Breusegem FV. 2018. Reactive oxygen species in plant development. Development **145**, dev164376.

Mhamdi A, Hager J, Chaouch S, *et al.* 2010. Arabidopsis GLUTATHIONE REDUCTASE1 plays a crucial role in leaf responses to intracellular hydrogen peroxide and in ensuring appropriate gene

expression through both salicylic acid and jasmonic acid signaling pathways. Plant Physiology **153**, 1144–1160.

Mittler R, Finka A, Goloubinoff P. 2012. How do plants feel the heat? Trends in Biochemical Sciences **37**, 118–125.

Nahar K, Hasanuzzaman M, Alam M, Fujita M. 2015. Exogenous glutathione confers high temperature stress tolerance in mung bean (Vigna radiata L.) by modulating antioxidant defense and methylglyoxal detoxification system. Environmental and Experimental Botany **112**, 44-54.

Noctor G. Queval G, Mhamdi A, Chaouch S, Foyer CH. 2011. Glutathione. Arabidopsis Book **9**, e0142. doi: 10.1199/tab.0142.

Noctor G, Reichheld J-P, Foyer CH. 2018. ROS-related redox regulation and signaling in plants. Seminars in Cell & Developmental Biology, **80**, 3-12.

Ohkama-Ohtsu N, Radwan S, Peterson A, Zhao P, Badr AF, Xiang C, Oliver DJ. 2007. Characterization of the extracellular gamma-glutamyl transpeptidases, GGT1 and GGT2, in *Arabidopsis*. The Plant Journal **49**, 865–77.

Parisy V, Poinssot B, Owsianowski L, Buchala A, Glazebrook J, Mauch F. 2007. Identification of PAD2 as a gamma-glutamylcysteine synthetase highlights the importance of glutathione in disease resistance of Arabidopsis. The Plant Journal **49**, 159–172.

Passaia G, Queval G, Bai J, Margis-Pinheiro M, Foyer CH. 2014. The effects of redox controls mediated by glutathione peroxidases on root architecture in Arabidopsis thaliana. Journal of Experimental Botany **65**, 1403-1413.

Portis AR Jr. 2003. Rubisco activase - Rubisco's catalytic chaperone. Photosynthesis Research **75**, 11-27.

Queval G, Issakidis-Bourguet E, Hoeberichts FA, Vandorpe M, Gakière B, Vanacker H, Miginiac-Maslow M, Van Breusegem F, Noctor G. 2007. Conditional oxidative stress responses in the Arabidopsis photorespiratory mutant cat2 demonstrate that redox state is a key modulator of daylength-dependent gene expression, and define photoperiod as a crucial factor in the regulation of H2O2-induced cell death. The Plant Journal **52**, 640–657.

Rahman I, Kode A, Biswas SK. 2006. Assay for quantitative determination of glutathione and glutathione disulfide levels using enzymatic recycling method. Nature Protocols **1**, 3159–3165.

Reed JW, Nagpal P, Poole DS, Furuya M, Chory J. 1993. Mutations in the gene for the red/far-red light receptor phytochrome B alter cell elongation and physiological responses throughout Arabidopsis development. The Plant Cell **5**, 147–157.

Reichheld J-P, Khafif M, Riondet C, Droux M, Bonnard G, Meyer Y. 2007. Inactivation of thioredoxin reductases reveals a complex interplay between thioredoxin and glutathione pathways in *Arabidopsis* development. The Plant Cell **19**, 1851–1865.

Riondet C, Desouris JP, Montoya JG, Chartier Y, Meyer Y, Reichheld J-P. 2012. A dicotyledon-specific glutaredoxin GRXC1 family with dimer-dependent redox regulation is functionally redundant with GRXC2. Plant, Cell and Environment **35**, 360–373.

Rodrigues O, Reshetnyak G, Grondin A, Saijo Y, Leonhardt N, Maurel C, Verdoucq L. 2017. Aquaporins facilitate hydrogen peroxide entry into guard cells to mediate ABA- and pathogen-triggered stomatal closure. Proceedings of the National Academy of Sciences **114**, 9200–9205.

Sato S, Kamiyama M, Iwata T, Makita N, Furukawa H, Ikeda H. 2006. Moderate increase of mean daily temperature adversely affects fruit set of Lycopersicon esculentum by disrupting specific physiological processes in male reproductive development. Annals in Botany. **97**, 731-8.

Schnaubelt D, Queval G, Dong Y, Diaz-Vivancos P, Makgopa ME, Howell G, Simone AD, Bai J, Hannah MA, Foyer CH. 2015. Low glutathione regulates gene expression and the redox potentials of the nucleus and cytosol in Arabidopsis thaliana. Plant Cell and Environment, **38**, 266-277.

Schwarzländer M, Fricker MD, Müller C, Marty L, Brach T, Novak J, Sweetlove LJ, Hell R, Meyer AJ. 2008. Confocal imaging of glutathione redox potential in living plant cells. Journal of Microscopy **231**, 299–316.

Shanmugam V, Tsednee M, Yeh K-C. 2012. ZINC TOLERANCE INDUCED BY IRON 1 reveals the importance of glutathione in the cross-homeostasis between zinc and iron in Arabidopsis thaliana. The Plant Journal **69**, 1006–1017.

Sumesh KV, Sharma-Natu P, Ghildiyal MC. 2008. Starch synthase activity and heat shock protein in relation to thermal tolerance of developing wheat grains. Biologia Plantarum **52**, 749-753.

Sun J, Qi L, Li Y, Chu J, Li C. 2012. PIF4-mediated activation of YUCCA8 expression integrates temperature into the auxin pathway in regulating arabidopsis hypocotyl growth. PLoS genetics **8**, e1002594.

Sylvestre-Gonon E, Schwartz M, Girardet J-M, Hecker A, Rouhier N. 2020 Is there a role for tau glutathione transferases in tetrapyrrole metabolism and retrograde signalling in plants? Philosophical Transactions Royal Society B **375**, 20190404. http://dx.doi.org/10.1098/rstb.2019.0404.

Toh S, Imamura A, Watanabe A, *et al.* 2008. High temperature-induced abscisic acid biosynthesis and its role in the inhibition of gibberellin action in Arabidopsis seeds. Plant Physiology **146**, 1368-85.

Trujillo-Hernandez JA, Bariat L, Enders TA, Strader LC, Reichheld J-P, Belin C. 2020. A Glutathione-dependent control of IBA pathway supports Arabidopsis root system adaptation to phosphate deprivation. Journal of Experimental Botany, **71**, 4843-4857.

Tsukagoshi H, Busch W, Benfey PN. 2010. Transcriptional regulation of ROS controls transition from proliferation to differentiation in the root. Cell **143**, 606–616.

Ugalde JM, Aller I, Kudrjasova L, *et al.* 2022. Endoplasmic reticulum oxidoreductin provides resilience against reductive stress and hypoxic conditions by mediating luminal redox dynamics. The Plant Cell. **34**, 4007-4027.

Vernoux T, Wilson RC, Seeley KA *et al*. 2000. The ROOT MERISTEMLESS1/CADMIUM SENSITIVE2 Gene Defines a Glutathione-Dependent Pathway Involved in Initiation and Maintenance of Cell Division during Postembryonic Root Development. The Plant Cell **12**, 97–110.

Volkov RA, Panchuk II, Mullineaux PM, Schöffl F. 2006. Heat stress-induced H(2)O(2) is required for effective expression of heat shock genes in Arabidopsis. Plant Molecular Biology **61**, 733–746.

Wickham H. 2016. ggplot2: Elegant Graphics for Data Analysis. Springer-Verlag New York. ISBN 978-3-319-24277-4, https://ggplot2.tidyverse.org.

Willems P, Mhamdi A, Stael S, Storme V, Kerchev P, Noctor G, Gevaert K, Van Breusegem F. 2016. The ROS Wheel: Refining ROS Transcriptional Footprints. Plant Physiology **171**, 1720–1733.

Wu Q, Lin J, Liu JZ, *et al.* 2012. Ectopic expression of Arabidopsis glutaredoxin AtGRXS17 enhances thermotolerance in tomato. Plant Biotechnology Journal **10**, 945-55.

Wu F, Chi Y, Jiang Z, *et al.* 2020. Hydrogen peroxide sensor HPCA1 is an LRR receptor kinase in Arabidopsis. Nature **578**, 577–581.

Yeh C-H, Kaplinsky NJ, Hu C, Charng Y-Y. 2012. Some like it hot, some like it warm/Phenotyping to explore thermotolerance diversity. Plant Science **195**, 10-23.

Zandalinas SI, Fritschi FB, Mittler R. 2020. Signal transduction networks during stress combination. Journal of Experimental Botany **71**, 1734-1741.

Figure legends

Figure 1: *In vivo* monitoring of the glutathione redox state upon heat stress. (A-D), GRX1-roGFP2 fluorescence ratio (left side) calculated from confocal images (right side) of cotyledon (A and C) or root apex (B and D) cells of ten-day-old Arabidopsis wild-type seedlings stably expressing the GRX1-roGFP2 construct and subjected to 27°C (A and B) or 37°C (C and D). roGFP2 fluorescence was collected at 505-530 nm after excitation with either 405 nm or 488 nm. Ratio images were calculated as the 405/488 nm fluorescence. Control samples were immersed in MS/2 liquid medium and observed at 20°C. Then, the temperature of the thermostatic chamber was increased and the roGFP2 fluorescence was monitored every 10-15 min for 1 hour. Scale bars = 50 µm. The data are representative of one experiment among three which gave similar data. Asterisks indicate a significant difference calculated by Student's t-test (* $P \leq 0.05$, ** $P \leq 0.01$) between 27°C/37°C and 20°C treatments. Means +/- SD are shown (n>6). (E), To fully reduce or oxidize the sensor, seedlings were immersed in 10 mM DTT or 100 mM H_2O_2, respectively. False colors indicate the fluorescence ratio on a scale from blue (reduced) to red (oxidized). (F), Monitoring of the cytosolic and nuclear roGFP2 redox ratio upon high temperatures. The fluorescence ratios were calculated from samples shown in Figures 1A, 1C and 1E. ROI containing nuclei (grey bars) or cytosol (black bars) were selected from confocal images of cotyledon cells subjected to 27°C or 37°C. Asterisks indicate a significant difference calculated by Student's t-test (* $P \leq 0.05$) between nuclear and cytosolic ratios. Means +/- SD are shown (n>6).

Figure 2: Measurement of glutathione levels upon heat stress. (A-B), Total extractible glutathione was measured in ten-day-old Arabidopsis wild-type seedlings subjected to 27 ° C

(A) or 37 ° C (B). Reduced and oxidized glutathione levels are indicated by white and grey bars, respectively. GSH/(GSH+GSSG) ratios are indicated above each bar. Asterisks indicate a significant difference (* P ≤ 0.05, ** P ≤ 0.01) between reduced (inside white bars) or total (above bars) glutathione levels between untreated plants (T0) and high temperature treated plants. No significant difference was observed in oxidized glutathione levels. The data are representative of one experiment among three which gave similar data. Means +/- SD are shown (n=3). Notice that the T0 time points are the same in (A) and (B). (C), Global protein S-glutathionylation upon high temperatures. Representative western-blot analysis (upper panel) of the S-glutathionylated proteins in total protein extracts. Total proteins extracted from ten-day-old Arabidopsis wild-type (Col-0) seedlings subjected to 27°C or 37°C run on non-reducing SDS-PAGE and total glutathione was detected with an anti-glutathione antibody (1:1000) by western-blot. Total protein staining with Coomassie blue is shown as a loading control. The intensity of each line (lower panel) was quantified using ImageJ and means +/- SD of 3 replicates are shown. (D), Quantification of the extractible GST activity on total protein extracts described in (C). (C,D), Asterisks indicate a significant difference calculated by Student's t-test (* P ≤ 0.05, ** P ≤ 0.01, and *** P ≤ 0.001) between 27°C/37°C and 20°C treatments. Means +/- SD are shown (n=3).

Figure 3: Glutathione level and roGFP2 redox ratio in the *cad2* low glutathione mutant. (A), Total extractible glutathione was measured in ten-day-old Arabidopsis wild-type (Col-0) and *cad2* seedlings at 20 ° C (white bars) or subjected to 27 ° C (grey bars) or 37 ° C (black bars) for indicated times. Asterisks indicate a significant difference calculated by Student's t-test (* P ≤ 0.05, ** P ≤ 0.01) between 27°C/37°C and 20°C treatments in *cad2*. Error bars represent SD (n = 3). (B-D), roGFP2 fluorescence ratio calculated from confocal images of

cotyledon epidermic cells of ten-day-old Arabidopsis Col-0 (filled bars, same data as in figure 1A and C) and *cad2* (hatched bars) seedlings stably expressing the GRX1-roGFP2 construct. (B) To fully reduce or oxidize the sensor, seedlings were immersed at 20°C in 10 mM DTT or 100 mM H_2O_2, respectively (white bars). (C-D) roGFP2 redox ratio was measured in plants subjected to 37 ° C (C, black bars) or 27 ° C (D, grey bars). The roGFP2 fluorescence was collected at 505-530 nm after excitation with either 405 nm or 488 nm. Ratio images were calculated as the 405/488 nm fluorescence. The data are representative of one experiment among two which gave similar data. Asterisks indicate a significant difference calculated by Student's t-test (* $P \leq 0.05$, ** $P \leq 0.01$) between 27°C/37°C and 20°C treatments. Means +/- SD are shown (n>6).

Figure 4: Low glutathione impairs thermotolerance. (A-C), Wild-type plants (Col-0), *cad2, pad2, gr1, grxc1, grxc2, grxc3, grxc4, gsnor-1, nox1, cat2* and Heat Shock Factor A1 quadruple knockout mutant (*hsfa1QK*) were subjected to a Thermotolerance to Moderate High Temperature (TMHT) regime. (A), TMHT design. (B), Pictures of the plates taken 11 days after recovery. (C), The viability of the plants is assessed by the recovery of shoot growth. (D), Viability rate of Col-0 plants grown on increasing concentrations of BSO. Lower panels show pictures of the plates after recovery from the TMHT treatment (37°C) or from untreated plants (20°C). Data are means of at least three biological repetitions +/- SD, n=30 to 100. Groups sharing the same letter are not significantly different from each other ($P \leq 0.01$, one-way ANOVA followed by a post hoc Tukey's honestly significant difference test (HSD)).

Figure 5: Low glutathione impairs thermomorphogenesis. (A-C), Wild-type plants (Col-0) and *cad2, pad2, gr1, grxc1, grxc2, grxc3, grxc4* and *grxs17* mutants were subjected to a 27°C thermomorphogenesis assay. (A), Thermomorphogenesis assay design. (B), Pictures of representative plants taken after 11 days of treatment. Black bar = 10mm. (C,D), Hypocotyl length measurements. Pictures of plants were taken, and the hypocotyl length of more than 30 plants per condition was measured using the Neuron J plugin from the ImageJ software. Groups sharing the same letter are not significantly different from each other ($P \leq 0.01$, one-way Kruskal-Wallis ANOVA (non-parametric) followed by a Pairwise Wilcoxon test).

Figure 6: Genome-wide analysis of *cad2* response to 27°C temperature. (A), Venn diagram of upregulated and downregulated genes at 2 h and 24 h (fold change cutoff log2>1, Paj<0.05) after the temperature shift in wild-type (Col-0) and *cad2* mutant. (B), Cutoff Gene ontologies (GO) characterize the biological processes enriched among the temperature-regulated genes that are shared or that are specific between the wild-type and the *cad2* mutant. (C-D), Heatmaps of upregulated (C) or downregulated (D) genes in the three RNAseq biological repetitions (1,2,3) before and after high temperature shift. Genes were clustered as follows: a, Col-0 27°C 2h; b, Col-0 27°C 24h; c, *cad2* 27°C 2h; d, *cad2* 27°C 24h; e, common Col-0 27°C 2h and Col-0 27°C 24h; f, common Col-0 27°C 2h and *cad2* 27°C 2h; g, common Col-0 27°C 24h and *cad2* 27°C 2h; h, common Col-0 27°C 24h and *cad2* 27°C 24h; i, common *cad2* 27°C 2h and *cad2* 27°C 24h; j, common Col-0 27°C 2h, Col-0 27°C 24h and *cad2* 27°C 2h; k, Col-0 27°C 2h, *cad2* 27°C 2h and *cad2* 27°C 24h; l, common Col-0 27°C 2h, Col-0 27°C 24h and *cad2* 27°C 24h; m, common Col-0 27°C 24h, *cad2* 27°C 2h and *cad2* 27°C 24h; n, common for all.

Figure 7: Genome-wide analysis of *cad2* response to 37°C temperature. (A), Venn diagram of upregulated and downregulated genes at 2 h and 24 h (fold change cutoff log2>1,

Paj<0.05) after the temperature shift in wild-type (Col-0) and *cad2* mutant. (B), Cutoff Gene ontologies (GO) characterize the biological processes enriched among the temperature-regulated genes that are shared or that are specific between the wild-type and the *cad2* mutant. (C-D), Heatmaps of upregulated (C) or downregulated (D) genes in the three RNAseq biological repetitions (1,2,3) before and after high temperature shift. Genes were clustered as follows: a, Col-0 37°C 2h; b, Col-0 37°C 24h; c, *cad2* 37°C 2h; d, *cad2* 37°C 24h; e, common Col-0 37°C 2h and Col-0 37°C 24h; f, common Col-0 37°C 2h and *cad2* 37°C 2h; g, common Col-0 37°C 24h and *cad2* 37°C 2h; h, common Col-0 37°C 24h and *cad2* 37°C 24h; i, common *cad2* 37°C 2h and *cad2* 37°C 24h; j, common Col-0 37°C 2h, Col-0 37°C 24h and *cad2* 37°C 2h; k, Col-0 37°C 2h, *cad2* 37°C 2h and *cad2* 37°C 24h; l, common Col-0 37°C 2h, Col-0 37°C 24h and *cad2* 37°C 24h; m, common Col-0 37°C 24h, *cad2* 37°C 2h and *cad2* 37°C 24h; n, common for all.

Figure 8: Glutathione-related gene expression upon high temperature. (A), Heatmap of glutathione-related genes (listed in Supplementary Table 1) expression in Col-0 and *cad2* under high temperature regimes, as compared to 20°C. Arrows highlight differentially expressed clusters at 27°C (blue) or 37°C (orange). (B), Differentially expressed genes selected from RNAseq data. Hashtags indicate a significant difference calculated by Student's t-test ($^{\#}$ P ≤ 0.05, $^{\#\#}$ P ≤ 0.01, and $^{\#\#\#}$ P ≤ 0.001) between 27°C/37°C and 20°C treatments in Col-0. Asterisks indicate a significant difference calculated by Student's t-test (* P ≤ 0.05, ** P ≤ 0.01, and *** P ≤ 0.001) between *cad2* / *pad2* and Col-0 at the same temperature and timepoint. Means +/- SD are shown (n=3).

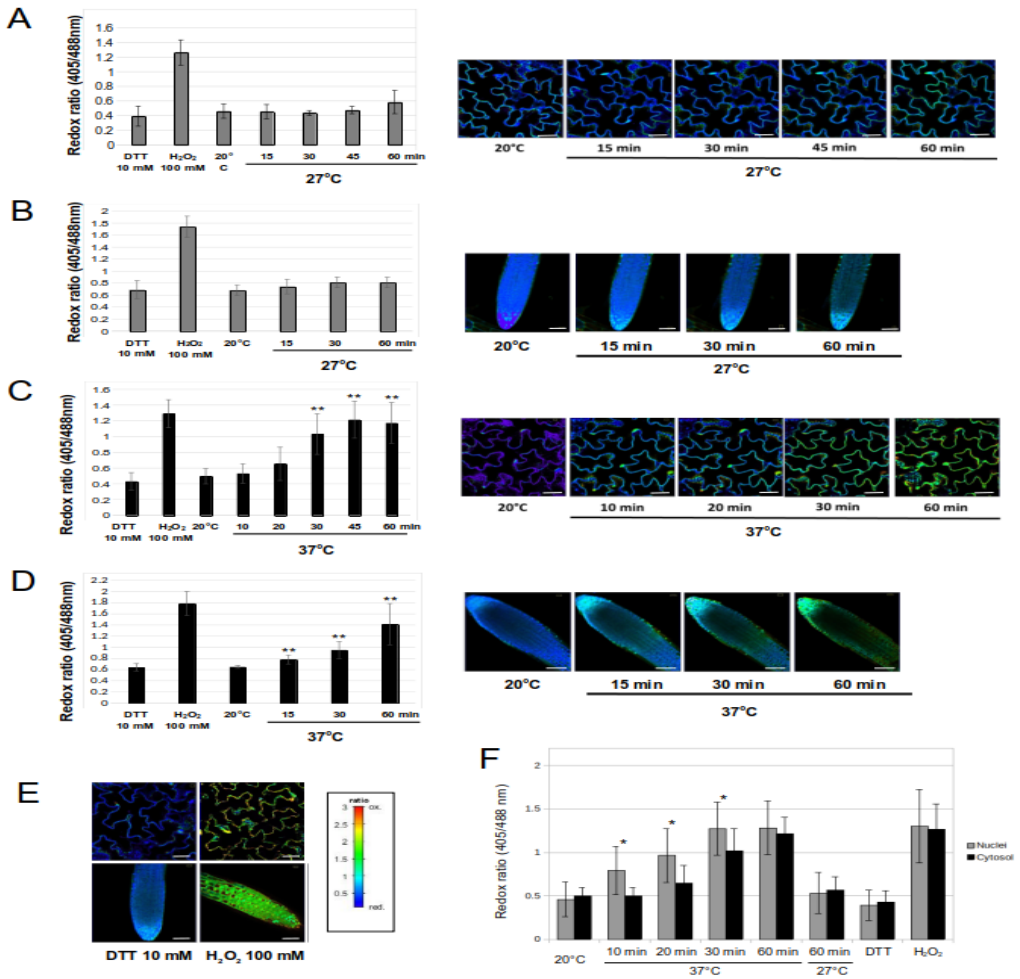

Figure 1: *In vivo* monitoring of the glutathione redox state upon heat stress. (A-D), GRX1-roGFP2 fluorescence ratio (left side) calculated from confocal images (right side) of cotyledon (A and C) or root apex (B and D) cells of ten-day-old Arabidopsis wild-type seedlings stably expressing the GRX1-roGFP2 construct and subjected to 27°C (A and B) or 37°C (C and D). roGFP2 fluorescence was collected at 505-530 nm after excitation with either 405 nm or 488 nm. Ratio images were calculated as the 405/488 nm fluorescence. Control samples were immersed in MS/2 liquid medium and observed at 20°C. Then, the temperature of the thermostatic chamber was increased and the roGFP2 fluorescence was monitored every 10-15 min for 1 hour. Scale bars = 50 µm. The data are representative of one experiment among three which gave similar data. Asterisks indicate a significant difference calculated by Student's t-test (* $P \leq 0.05$, ** $P \leq 0.01$) between 27°C/37°C and 20°C treatments. Means +/- SD are shown (n>6). (E), To fully reduce or oxidize the sensor, seedlings were immersed in 10 mM DTT or 100 mM H_2O_2, respectively. False colors indicate the fluorescence ratio on a scale from blue (reduced) to red (oxidized). (F), Monitoring of the cytosolic and nuclear roGFP2 redox ratio upon high temperatures. The fluorescence ratios were calculated from samples shown in Figures 1A, 1C and 1E. ROI containing nuclei (grey bars) or cytosol (black bars) were selected from confocal images of cotyledon cells subjected to 27°C or 37°C. Asterisks indicate a significant difference calculated by Student's t-test (* $P \leq 0.05$) between nuclear and cytosolic ratios. Means +/- SD are shown (n>6).

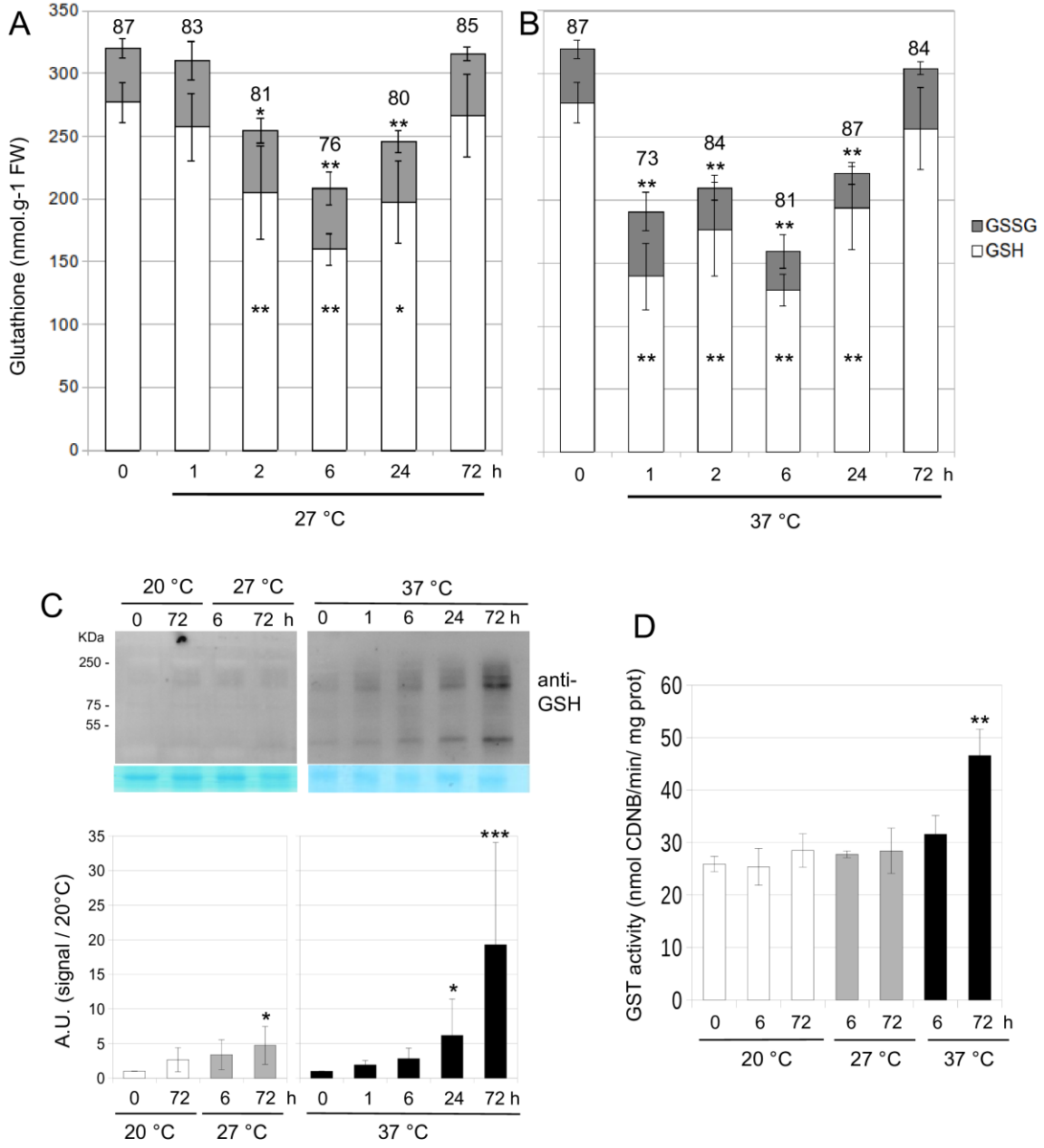

Figure 2: Measurement of glutathione levels upon heat stress. (A-B), Total extractible glutathione was measured in ten-day-old Arabidopsis wild-type seedlings subjected to 27 ° C (A) or 37 ° C (B). Reduced and oxidized glutathione levels are indicated by white and grey bars, respectively. GSH/(GSH+GSSG) ratios are indicated above each bar. Asterisks indicate a significant difference (* P ≤ 0.05, ** P ≤ 0.01) between reduced (inside white bars) or total (above bars) glutathione levels between untreated plants (T0) and high temperature treated plants. No significant difference was observed in oxidized glutathione levels. The data are representative of one experiment among three which gave similar data. Means +/- SD are shown (n=3). Notice that the T0 time points are the same in (A) and (B). (C), Global protein S-glutathionylation upon high temperatures. Representative western-blot analysis (upper panel) of the S-glutathionylated proteins in total protein extracts. Total proteins extracted from ten-day-old Arabidopsis wild-type (Col-0) seedlings subjected to 27ºC or 37ºC run on non-reducing SDS-PAGE and total glutathione was detected with an anti-glutathione antibody (1:1000) by western-blot. Total protein staining with Coomassie blue is shown as a loading control. The intensity of each line (lower panel) was quantified using ImageJ and means +/- SD of 3 replicates are shown. (D), Quantification of the extractible GST activity on total protein extracts described in (C). (C,D), Asterisks indicate a significant difference calculated by Student's t-test (* P ≤ 0.05, ** P ≤ 0.01, and *** P ≤ 0.001) between 27ºC/37ºC and 20ºC treatments. Means +/- SD are shown (n=3).

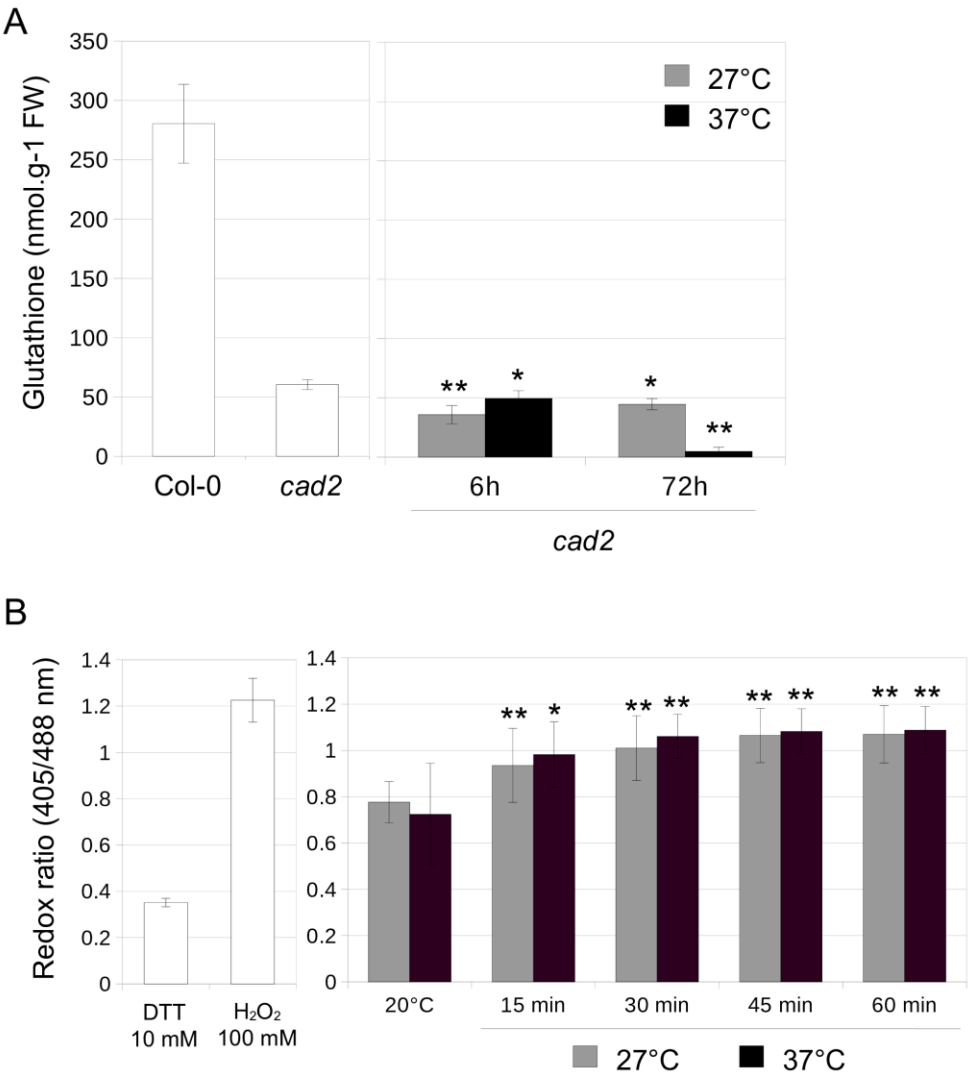

Figure 3: Glutathione level and roGFP2 redox ratio in the *cad2* low glutathione mutant. (A), Total extractible glutathione was measured in ten-day-old Arabidopsis wild-type (Col-0) and *cad2* seedlings at 20 ° C (white bars) or subjected to 27 ° C (grey bars) or 37 ° C (black bars) for indicated times. Asterisks indicate a significant difference calculated by Student's t-test (* $P \leq 0.05$, ** $P \leq 0.01$) between 27°C/37°C and 20°C treatments in *cad2*. Error bars represent SD (n = 3). (B), roGFP2 fluorescence ratio calculated from confocal images of cotyledon epidermic cells of ten-day-old Arabidopsis *cad2* seedlings stably expressing the GRX1-roGFP2 construct and subjected to 27 ° C (grey bars) or 37 ° C (black bars). The roGFP2 fluorescence was collected at 505-530 nm after excitation with either 405 nm or 488 nm. Ratio images were calculated as the 405/488 nm fluorescence. To fully reduce or oxidize the sensor, seedlings were immersed in 10 mM DTT or 100 mM H_2O_2, respectively (white bars). The data are representative of one experiment among two which gave similar data. Asterisks indicate a significant difference calculated by Student's t-test (* $P \leq 0.05$, ** $P \leq 0.01$) between 27°C/37°C and 20°C treatments. Means +/- SD are shown (n>6).

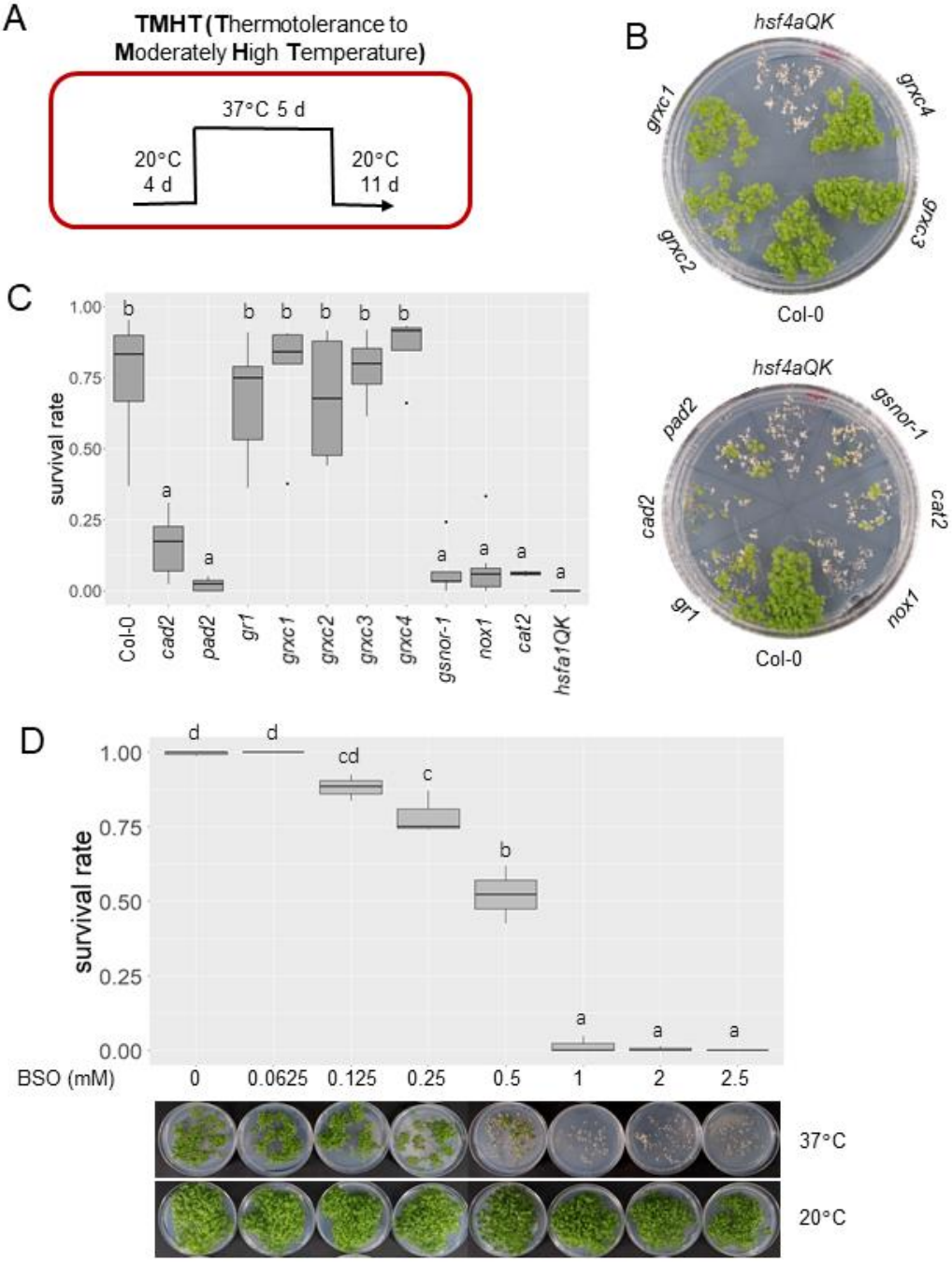

Figure 4: Low glutathione impairs thermotolerance. (A-C), Wild-type plants (Col-0), *cad2, pad2, gr1, grxc1, grxc2, grxc3, grxc4, gsnor-1, nox1, cat2* and Heat Shock Factor A1 quadruple knockout mutant (*hsfa1QK*) were subjected to a Thermotolerance to Moderate High Temperature (TMHT) regime. (A), TMHT design. (B), Pictures of the plates taken 11 days after recovery. (C), The viability of the plants is assessed by the recovery of shoot growth. (D), Viability rate of Col-0 plants grown on increasing concentrations of BSO. Lower panels show pictures of the plates after recovery from the TMHT treatment (37°C) or from untreated plants (20°C). Data are means of at least three biological repetitions +/- SD, n=30 to 100. Groups sharing the same letter are not significantly different from each other ($P \leq 0.01$, one-way ANOVA followed by a post hoc Tukey's honestly significant difference test (HSD)).

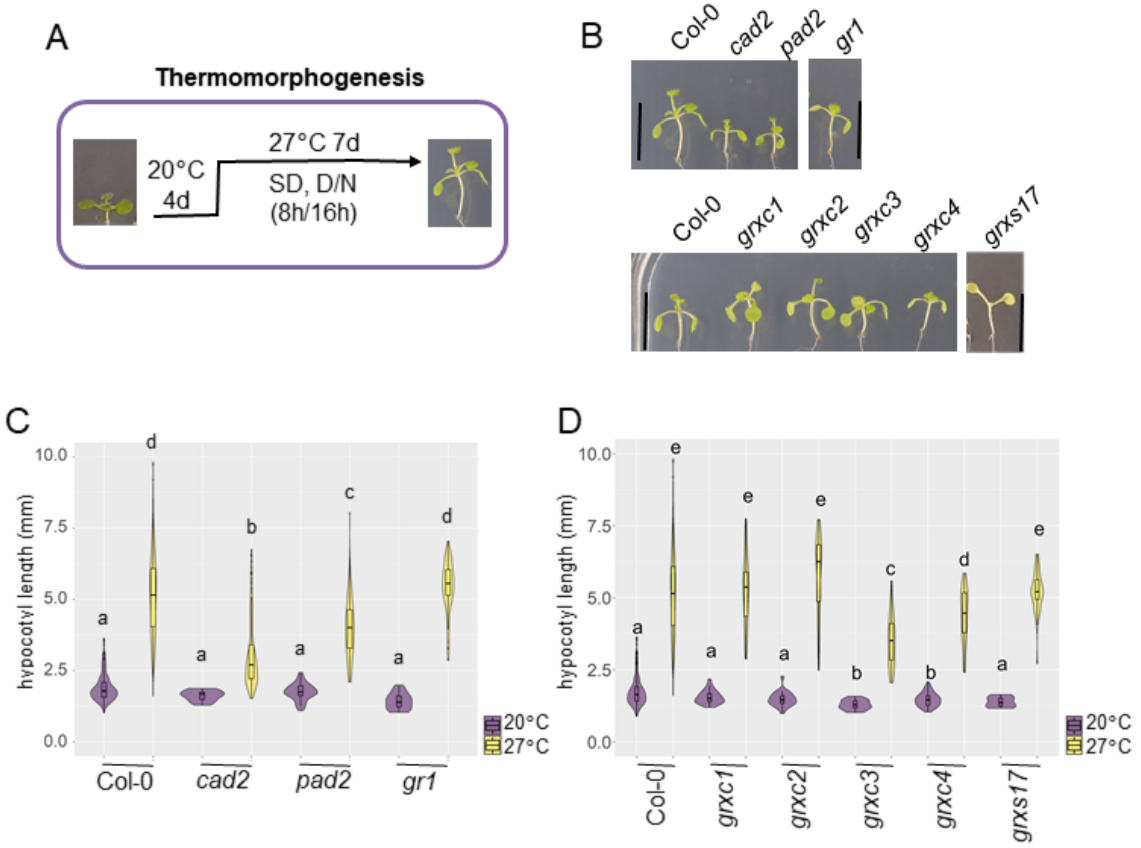

Figure 5: Low glutathione impairs thermomorphogenesis. (A-C), Wild-type plants (Col-0) and *cad2, pad2, gr1, grxc1, grxc2, grxc3, grxc4* and *grxs17* mutants were subjected to a 27°C thermomorphogenesis assay. (A), Thermomorphogenesis assay design. (B), Pictures of representative plants taken after 11 days of treatment. Black bar = 10mm. (C,D), Hypocotyl length measurements. Pictures of plants were taken, and the hypocotyl length of more than 30 plants per condition was measured using the Neuron J plugin from the ImageJ software. Groups sharing the same letter are not significantly different from each other ($P \leq 0.01$, one-way Kruskal-Wallis ANOVA (non-parametric) followed by a Pairwise Wilcoxon test).

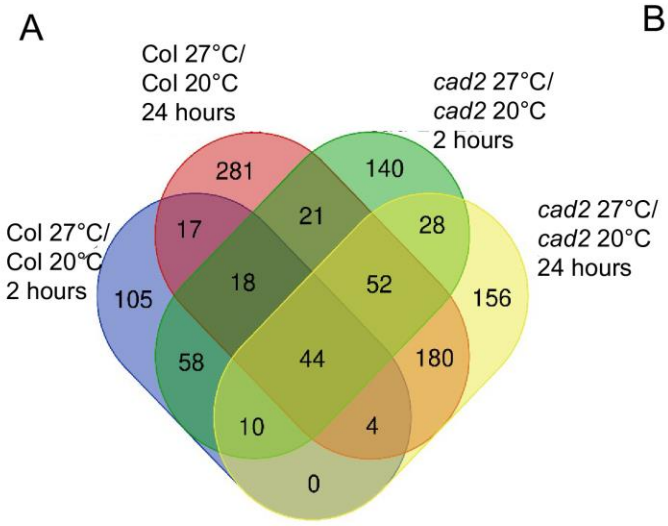

B

GO category	p-value
Col specific	
Response to chemical stimulus	9.05^{e}-8
Response to stimulus	2.3^{e}-6
Response to stress	8.5^{e}-5
Response to endogenous stimulus	1.0^{e}-4
Response to oxidative stress	1.8^{e}-4
cad2 specific	
Response to stimulus	1.1^{e}-19
Response to stress	2.2^{e}-18
Response to inorganic substance	6.6^{e}-15
Response to chemical stimulus	2.2^{e}-13
Response to oxidative stress	1.5^{e}-12
Common	
Response to stimulus	2.2^{e}-20
Response to chemical stimulus	5.5^{e}-17
Response to stress	8.2^{e}-15
Response to heat	2.1^{e}-11
Response to temperature stimulus	4.3^{e}-11

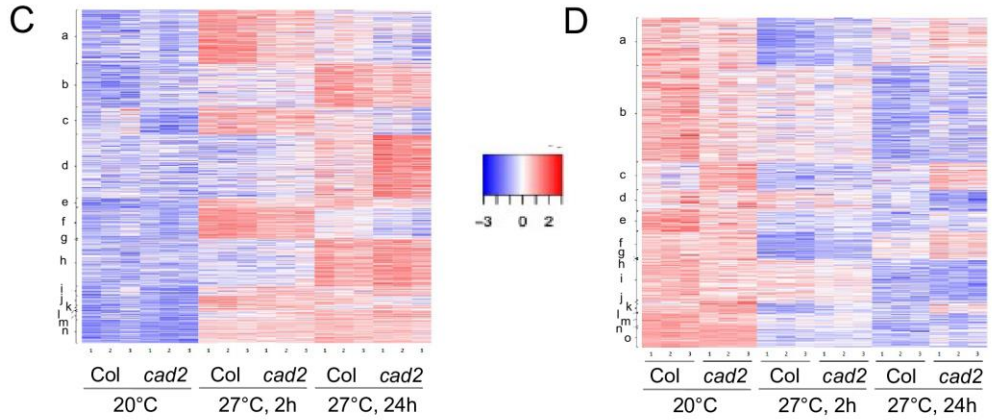

Figure 6: Genome-wide analysis of *cad2* response to 27°C temperature. (A), Venn diagram of upregulated and downregulated genes at 2 h and 24 h (fold change cutoff log2>1, Paj<0.05) after the temperature shift in wild-type (Col-0) and *cad2* mutant. (B), Cutoff Gene ontologies (GO) characterize the biological processes enriched among the temperature-regulated genes that are shared or that are specific between the wild-type and the *cad2* mutant. (C-D), Heatmaps of upregulated (C) or downregulated (D) genes in the three RNAseq biological repetitions (1,2,3) before and after high temperature shift. Genes were clustered as follows: a, Col-0 27°C 2h; b, Col-0 27°C 24h; c, *cad2* 27°C 2h; d, *cad2* 27°C 24h; e, common Col-0 27°C 2h and Col-0 27°C 24h; f, common Col-0 27°C 2h and *cad2* 27°C 2h; g, common Col-0 27°C 24h and *cad2* 27°C 2h; h, common Col-0 27°C 24h and *cad2* 27°C 24h; i, common *cad2* 27°C 2h and *cad2* 27°C 24h; j, common Col-0 27°C 2h, Col-0 27°C 24h and *cad2* 27°C 2h; k, Col-0 27°C 2h, *cad2* 27°C 2h and *cad2* 27°C 24h; l, common Col-0 27°C 2h, Col-0 27°C 24h and *cad2* 27°C 24h; m, common Col-0 27°C 24h, *cad2* 27°C 2h and *cad2* 27°C 24h; n, common for all.

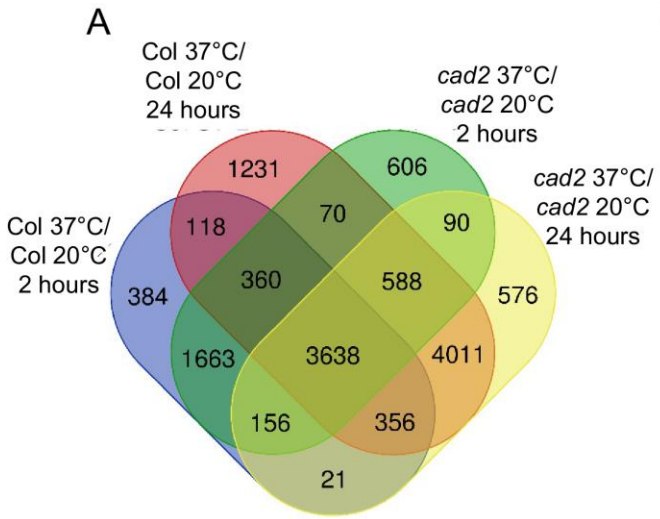

B

GO category	p-value
Col specific	
Post embryonic development	1.4^{e}-12
Multicellular organism developement	3.3^{e}-6
Reproductive developmental process	2.5^{e}-6
Multicellular organism process	1.1^{e}-5
Developmental process	2.1^{e}-5
cad2 specific	
Response to stimulus	2.1^{e}-5
Cation binding	5.6^{e}-6
Ion binding	5.6^{e}-6
Transition metal ion binding	8.5^{e}-6
Binding	1.2^{e}-5
Common	
Response to stimulus	1.8^{e}-28
Post embryonic development	1.3^{e}-19
Response to stress	3.7^{e}-18
Response to chemical stimulus	4.2^{e}-16
Response to abiotic stimulus	2.0^{e}-12

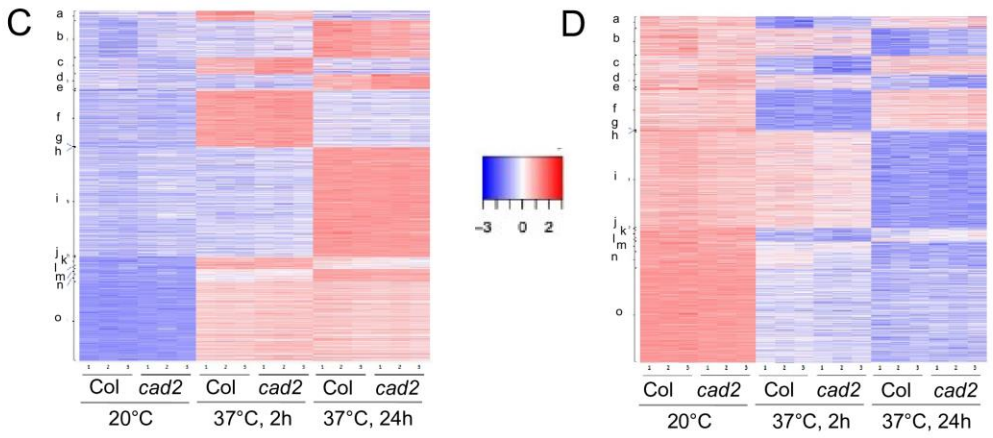

Figure 7: Genome-wide analysis of *cad2* response to 37°C temperature. (A), Venn diagram of upregulated and downregulated genes at 2 h and 24 h (fold change cutoff log2>1, Paj<0.05) after the temperature shift in wild-type (Col-0) and *cad2* mutant. (B), Cutoff Gene ontologies (GO) characterize the biological processes enriched among the temperature-regulated genes that are shared or that are specific between the wild-type and the *cad2* mutant. (C-D), Heatmaps of upregulated (C) or downregulated (D) genes in the three RNAseq biological repetitions (1,2,3) before and after high temperature shift. Genes were clustered as follows: a, Col-0 37°C 2h; b, Col-0 37°C 24h; c, *cad2* 37°C 2h; d, *cad2* 37°C 24h; e, common Col-0 37°C 2h and Col-0 37°C 24h; f, common Col-0 37°C 2h and *cad2* 37°C 2h; g, common Col-0 37°C 24h and *cad2* 37°C 2h; h, common Col-0 37°C 24h and *cad2* 37°C 24h; i, common *cad2* 37°C 2h and *cad2* 37°C 24h; j, common Col-0 37°C 2h, Col-0 37°C 24h and *cad2* 37°C 2h; k, Col-0 37°C 2h, *cad2* 37°C 2h and *cad2* 37°C 24h; l, common Col-0 37°C 2h, Col-0 37°C 24h and *cad2* 37°C 24h; m, common Col-0 37°C 24h, *cad2* 37°C 2h and *cad2* 37°C 24h; n, common for all.

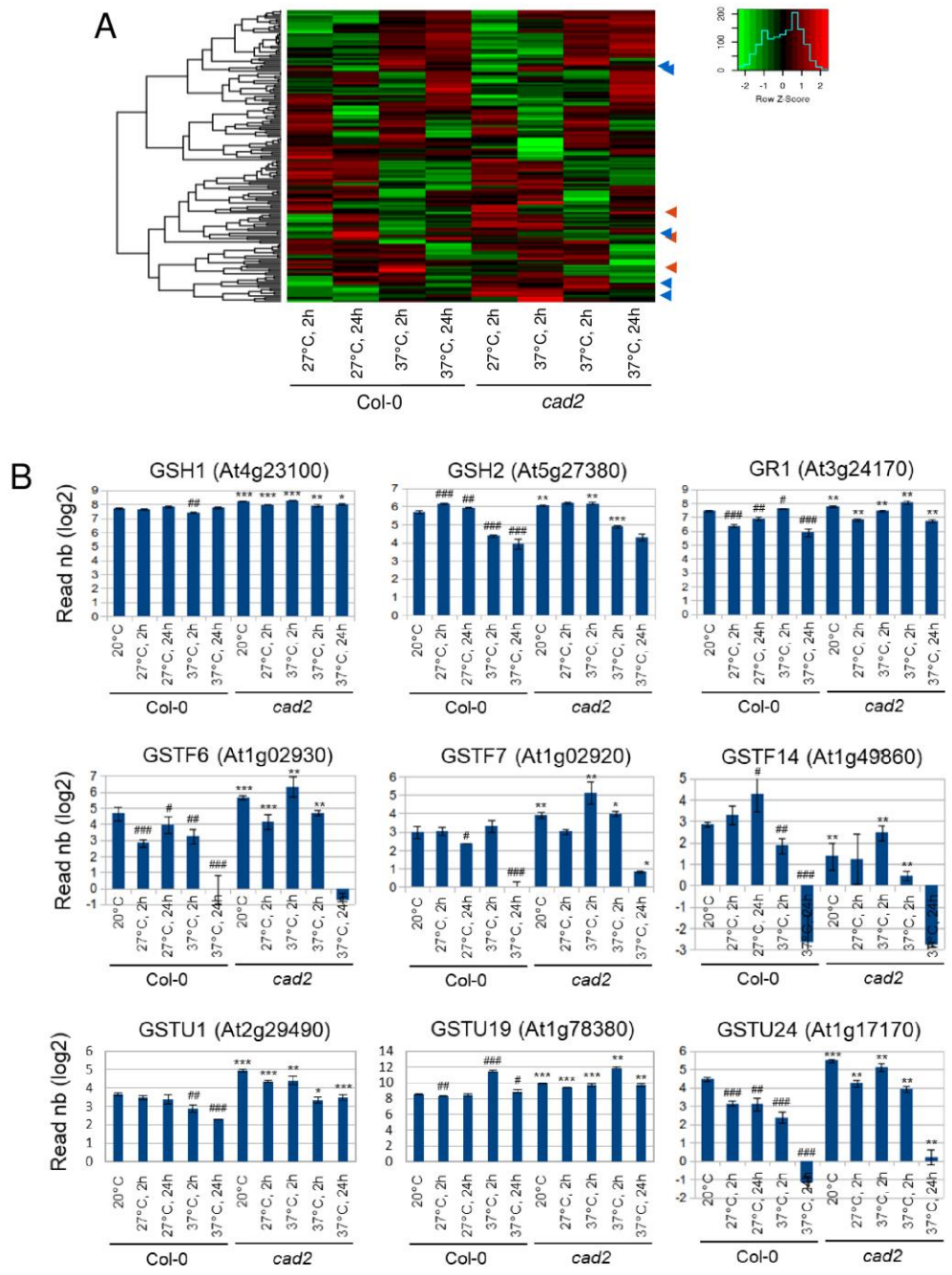

Figure 8: Glutathione-related gene expression upon high temperature. (A), Heatmap of glutathione-related genes (listed in Supplementary Table 1) expression in Col-0 and *cad2* under high temperature regimes, as compared to 20°C. Arrows highlight differentially expressed clusters at 27°C (blue) or 37°C (orange). (B), Differentially expressed genes selected from RNAseq data. Hashtags indicate a significant difference calculated by Student's t-test ($^{\#}$ P ≤ 0.05, $^{\#\#}$ P ≤ 0.01, and $^{\#\#\#}$ P ≤ 0.001) between 27°C/37°C and 20°C treatments in Col-0. Asterisks indicate a significant difference calculated by Student's t-test (* P ≤ 0.05, ** P ≤ 0.01, and *** P ≤ 0.001) between *cad2* / *pad2* and Col-0 at the same temperature and timepoint. Means +/- SD are shown (n=3).